SOVIET PHYSICS

USPEKHI

A Translation of Uspekhi Fizicheskikh Nauk

SOVIET PHYSICS USPEKHI (Russian Vol. 99, Nos. 1 and 2) MARCH-APRIL 1970

533.6 + 550.388

IONOSPHERIC AERODYNAMICS

A. V. GUREVICH, L. P. PITAEVSKIĬ, and V. V. SMIRNOVA

P. N. Lebedev Physics Institute, USSR Academy of Sciences; Institute of Physics Problems, USSR Academy of Sciences; Moscow Physicotechnical Institute

Usp. Fiz. Nauk 99, 3–49 (September, 1969)

I. INTRODUCTION

INTEREST in the problem of ionospheric aerodynamics, the theory of flow of a rarefied ionospheric plasma around moving bodies, has started to attract attention the instant the first artificial earth satellite was launched. The main results of the research in this field through 1964 were reported in the review[1] and in the monograph[2]. Since that time, essentially new results were obtained, and the present review is devoted to their description. Mention should be made here, first, of the response of the flow to the electric field due to the perturbation of the plasma by the body. We pay principal attention to this problem in this review.

For lack of space, we cannot discuss all the topics in which progress was made in recent years. For the reader's convenience, however, the bibliography contains also references to articles devoted to problems connected with flow around bodies, but not discussed in the review itself.

We start with the conditions that actually exist in the ionosphere in the region where the charged-particles concentration has a maximum. In this region the ion temperature is $T_i \sim 1000°K$ and the electron temperature[3] is $T_e \sim (1-2.5)\times 10^{3°}K$. At a body velocity $v_0 = 8 \times 10^5$ cm/sec, the Mach number turns out to be of the order of $b = (Mv_0^2/2T)^{1/2} \sim 8-6$, and it can be assumed that

$$b=\sqrt{\frac{Mv_0^2}{2T_e}} \gg 1 \qquad (1)$$

(here M is the ion mass); in the numerical estimate it is assumed that the ions are those of oxygen, O^+. It is noted that He^+ and H^+ ions are also encountered above 400 km, and are in the majority at altitudes exceeding 1000 km. This decreases the Mach number to $b \sim 1.2$. On the other hand,

$$\sqrt{\frac{mv_0^2}{2T_e}} \sim 5\cdot 10^{-2} \ll 1, \qquad (2)$$

where m is the electron mass, i.e., the velocities of the bodies are always much smaller than the thermal velocity of the electron.

The electron concentration is $N_e \sim 10^5-10^6$ cm^{-3}. The Debye radius is then

$$D=\left(\frac{T_e}{4\pi e^2 N_e}\right)^{1/2} \sim 0.1-0.5 \text{ cm}.$$

Therefore for real bodies in the ionosphere, with dimensions $R_0 \sim 1$ m, the following inequality is satisfied with sufficient margin

$$R_0 \gg D. \qquad (3)$$

As to the mean free path of the ions and electrons, at altitudes $h \gtrsim 150-200$ 1 km they are large, $l \sim 100$ m. Consequently, $l \gg R_0$ and the influence of collisions can be neglected in first approximation. We shall likewise disregard the influence of the magnetic field on the motion of the electrons and the ions. It is well known (see[2]) that this influence becomes appreciable at sufficiently large distances from the body ($z \gtrsim Mcv_0/eH$).

II. FUNDAMENTAL EQUATIONS AND SIMILARITY LAW

Neglect of collisions makes it possible to describe the problem with the aid of collisionless kinetic equations for the ion and electron distribution functions $f(\mathbf{r}, \mathbf{v})$ and $f_e(\mathbf{r}, \mathbf{v})$. In a coordinate frame connected with the moving body, the problem is stationary and the equation for the distribution function of the ions is

$$\mathbf{v}\frac{\partial f}{\partial \mathbf{r}} - \frac{e}{M}\frac{\partial \varphi}{\partial \mathbf{r}}\frac{\partial f}{\partial \mathbf{v}} = 0 \qquad (4)$$

(φ is the electric potential). The equation for f_e differs from (4) only in that the substitutions $M \to m$ and $e \to -e$ must be made. It is necessary to add to these equations also the Poisson equation

$$\Delta\varphi = -4\pi e\left(\int f\,d^3v - \int f_e\,d^3v\right). \qquad (5)$$

We simplify Eqs. (4) and (5) by using the inequality (1)–(3)[4]. We first use inequality (3) and take account

of the fact that the characteristic dimension of the inhomogeneity, which arises when the body moves, is R_0, and the characteristic potentials are $\sim T_e/e$. The left side of (5) is then of the order of T_e/eR_0^2, and the right side is of the order of $4\pi e(N_e - N_i)$. Their ratio is

$$\frac{T_e}{4\pi e^2 N R_0^2} \sim \left(\frac{D}{R_0}\right)^2. \quad (6)$$

This means that when condition (3) is satisfied it is possible to neglect the left side of (5) completely, and we can write in lieu of (5) the quasineutrality condition $N_e = N_i$, or

$$\int f_i d^3v = \int f_e d^3v. \quad (7)$$

This, however, calls for certain remarks. The point is that the quasi-neutrality is certainly violated in the immediate vicinity of the surface of the body. Near the surface there is a screening layer of thickness of the order of the Debye radius, in which the potential distribution depends on the boundary conditions on the body and on the potential of the body. By virtue of the condition (3), the thickness of this layer is in general small. It is important, however, that the plasma is strongly rarefied in the region behind the body, so that the Debye radius can be much larger than in the surrounding space. Here, in the "region of maximum rarefaction"[1,2], the deviations from quasineutrality are appreciable. Let us estimate the dimension l of this region behind a disc of radius R_0 placed in a plasma stream. The minimum density on the z axis behind the disc is of the order of (at $T_e = T_i$)

$$\frac{N_{\min}}{N} \sim \sqrt{b}\left(b + \frac{\pi}{2\sqrt{2}}\right) \exp\left(-\frac{\pi b}{\sqrt{2}}\right)$$

(see formula (73a) of Ch. IX). Therefore the dimension l is determined by the relation

$$l \sim \frac{D}{b^{1/4}\left(b + \frac{\pi}{2\sqrt{2}}\right)^{1/2}} \exp\left(\frac{\pi b}{2\sqrt{2}}\right), \quad D = \left(\frac{T_e}{4\pi e^2 N_0}\right)^{1/2}.$$

It follows therefore that under the conditions of the ionosphere $l \sim 0.5R_0$. We see that the maximum value of l is much larger than D, but still smaller than R_0. This means that in the greater part of the perturbed region the deviations from quasineutrality are small, although the dimensions of the maximum rarefaction region turn out to be quite appreciable.*

The transition from (5) and (7) leads to more than just an appreciable simplification of the calculations. Such a transition eliminates the electric charge e from the equations. Indeed, if we introduce in place of φ the dimensionless potential

$$\psi = \frac{e\varphi}{T_e}, \quad (8)$$

then the equation will no longer contain e. This changes greatly the dimensional character of the equations, since the natural parameter with the dimension of length, the Debye radius, disappears together with e.* All that remains in the problem are parameters characterizing the dimensions of the body. This causes, in particular, the picture of flow at a given velocity around bodies of similar shape to be similar. In addition, the relative concentration N/N_0 (where N_0 is the concentration of the unperturbed plasma) turns out to be independent of N_0.

We note also that the dimensional structure of Eqs. (4) and (7) turns out to be the same as in the equations of hydrodynamics of an ideal compressible liquid. This indicates that the fundamental phenomena may be similar in character to hydrodynamics.

We shall now use the condition (2)—the slowness of the body motion compared with the electron velocity. Under real conditions, the surface of the body usually has a negative potential φ_0. If

$$\exp\left(\frac{e\varphi_0}{T_e}\right) \ll 1,$$

then the electron current on the body is small and disturbs little the equilibrium of the electron gas. The electrons are then in equilibrium in all the regions of the plasma where the potential is negative and there are no potential wells. (Some of the electrons cannot enter a region where there are potential wells without collisions.) Actually this pertains to the entire perturbed region behind the body, where the electron density is thus given by the Boltzmann formula

$$N_e = N_0 \exp\left(\frac{e\varphi}{T_e}\right). \quad (9)$$

Substituting (9) in (7), we obtain a direct equation for φ in terms of f:

$$\varphi = \frac{T_e}{e} \ln\left(\frac{\int f d^3v}{N_0}\right). \quad (10)$$

Let us simplify, finally, Eq. (4) by using the "hypersonic" character of the motion of the body, as expressed by the inequality (1). If we choose the z axis along the direction of the incoming stream, then (4) takes the form

$$v_z \frac{\partial f}{\partial z} + \mathbf{v}_1 \frac{\partial f}{\partial \mathbf{r}_1} - \frac{e}{M}\frac{\partial \varphi}{\partial z}\frac{\partial f}{\partial v_z} - \frac{e}{M}\frac{\partial \varphi}{\partial \mathbf{r}_1}\frac{\partial f}{\partial \mathbf{v}_1} = 0,$$

where $\mathbf{r}_1$ and $\mathbf{v}_1$ are the projections of the vectors r and v on the plane perpendicular to the z axis. If condition (1) is satisfied, the perturbed region turns out to be elongated along the z axis. If its transverse dimension is $\sim R_0$, then its longitudinal dimension is of the order of bR_0. Therefore $|\partial\varphi/\partial \mathbf{r}_1| \gg \partial\varphi/\partial z$ and the term with $\partial\varphi/\partial z$ can be neglected. In addition, in the reference frame considered with the body we have $v_z \approx v_0$, i.e., the thermal scatter of the ions in the z direction can be neglected. We finally obtain

$$v_0 \frac{\partial f}{\partial z} + \mathbf{v}_1 \frac{\partial f}{\partial \mathbf{r}_1} - \frac{e}{M}\frac{\partial \varphi}{\partial \mathbf{r}_1}\frac{\partial f}{\partial \mathbf{v}_1} = 0. \quad (11)$$

This equation does not contain v_z at all. We can therefore introduce $\int f dv_z$ in place of f as the unknown function.

We change over directly to dimensionless variables.

*The case when the dimension of the region of maximum rarefaction is comparable with R_0 was considered in [2] (p. 127). It should be noted at the same time that N_{min} was calculated there without allowance for the influence of the electric field on motion of the ions, and this led to larger values of the rarefaction and greatly increased the dimensions of the region of maximum rarefaction.

* The fact that e drops out of the equations does not mean, of course, that the electric fields produced during the motion are negligible. To the contrary, the transition from (5) to (7) corresponds formally to the limit as $e \to \infty$.

We put*

$$\mathbf{v}_1 = \sqrt{\frac{2T_e}{M}}\,\mathbf{u}, \quad \mathbf{r}_1 = R_0\boldsymbol{\rho}, \quad z = tR_0 b, \quad b = \left(\frac{Mv_0^2}{2T_e}\right)^{1/2},$$
$$\int f\,dv_z = \frac{MN_0}{2\pi T_e}\,g(t, \boldsymbol{\rho}, \mathbf{u}), \quad \psi = \frac{e\varphi}{T_e}. \tag{12}$$

Substituting (12) in (11) and (7) we obtain a system of equations in which all the possible simplifications have been made.

$$\left.\begin{aligned} &\frac{\partial g}{\partial t} + \mathbf{u}\frac{\partial g}{\partial \boldsymbol{\rho}} - \frac{1}{2}\frac{\partial \psi}{\partial \boldsymbol{\rho}}\frac{\partial g}{\partial \mathbf{u}} = 0, \\ &\psi = \ln \int_{-\infty}^{\infty}\int g\,d^2u. \end{aligned}\right\} \tag{13}$$

Let us proceed to formulate the boundary conditions for the system (13). We assume that the surface of the body is such that all the ions falling on it recombine, i.e., they fly off in the form of neutral atoms. This corresponds, with sufficient accuracy, to the ordinary conditions on a metallic surface[5]. The condition for the absence of reflected ions,

$$f = 0 \quad \text{if} \quad \mathbf{nv} > 0 \tag{14}$$

(n—normal to the surface of the body) should then be satisfied on the surface of the body. We note first that the absence of reflected particles and the neglect of the velocity spread in the direction of z in (13) result in no perturbation at all in front of the body. If we place the origin at the most forward point of the body, this means

$$g = \exp\left(-\frac{Mv^2}{2T_i}\right) = \exp(-\beta u^2) \quad \text{if} \quad t < 0, \qquad \beta = \frac{T_e}{T_i}. \tag{15}$$

The boundary condition (14) is then rewritten in the dimensionless variables (12) in the form of a condition on the contour of the cross section of the body

$$g = 0 \quad \text{if} \quad \mathbf{n}_1\mathbf{u} > -n_z b,$$

where $\mathbf{n}_1$ is the normal to the contour of the section of the body in the plane t = const. Recognizing that $n_z b = \operatorname{cot}\alpha$, where α is the angle between the normal n to the surface and the t axis (in the coordinates ρ and t), we obtain ultimately

$$g = 0 \quad \text{if} \quad \mathbf{n}_1\mathbf{u} > -\operatorname{ctg}\alpha. \tag{16}$$

The cross section, of course, changes with t. For example, the contours of the cross section of a spherical body are circles of radius $r(t) = \{1 - b^2[t - (1/b)]^2\}^{1/2}$. In addition, at large distances from the body, the perturbations should decrease:

$$g \to \exp(-\beta u^2) \quad \text{as} \quad |\boldsymbol{\rho}|,\ t \to \infty. \tag{17}$$

An important simplification of the boundary conditions for not too strongly elongated bodies (i.e., bodies whose longitudinal dimension is of the order of the transverse one) is connected with the fact that in terms of the coordinates ρ and t the body becomes flattened by a factor $b = (Mv_0^2/2T_e)^{1/2}$. The ratio of the longitudinal dimension to the transverse one, in terms of the variables ρ and t, is of the order of 1/b. Therefore when $b \gg 1$ the body itself can be replaced by a plate coinciding with the maximal cross section of the body. Aligning, in addition, the origin t = 0 with the plane of the maximum cross section S, we rewrite the boundary conditions (15) and (16) as $t \to +0$ in the form

$$\left.\begin{aligned} &g = 0, \quad \text{if} \quad R_0\boldsymbol{\rho} \text{ lies inside } S; \\ &g = \exp(-\beta u^2), \quad \text{if} \quad R_0\boldsymbol{\rho} \text{ lies outside } S. \end{aligned}\right\} \tag{18}$$

The physical meaning of (13) with boundary condition (18) is clear: they determine how the ions fill, in a time t, an empty region equal to the maximum cross section of the value S in the plane ρ. This should be the situation in the case of large Mach numbers $b \gg 1$: the rapidly moving body absorbed all the ions in a cylindrical region with a transverse dimension equal to the maximum cross section of the body, after which this region becomes filled with plasma*.

It should be borne in mind that the discontinuous character of the boundary conditions (18) leads to a singularity in the last terms of the Eq. (13) at t = 0 at the points ρ_0 lying on the contour of the maximum cross section of the body. Let us therefore pay special attention to the vicinity of the singularity points. We put $\xi = \mathbf{n}_1(\boldsymbol{\rho}_0 - \boldsymbol{\rho})$ (where $\mathbf{n}_0$ is the normal to the cross section S at the point of the contour ρ_0), and we consider small values of ξ and t:

$$|\xi| \ll 1, \qquad t \ll 1. \tag{19}$$

When the condition (19) is satisfied we can neglect the curvature of the contour near the point ρ_0. In addition, the ions flowing around the other edge of the body do not have time to fall on the observation point. The problem then has no characteristic spatial dimension. In this case the solution of (13) can depend only on the ratio ξ/t, i.e., the motion is self-similar. Putting

$$g_a(\tau, u_\xi) = \frac{1}{\sqrt{\pi}}\int_{-\infty}^{\infty} g(\tau, u_\xi, u_\eta)\,du_\eta, \qquad \tau = \frac{\xi}{t}, \qquad u_\xi = \mathbf{u}\mathbf{n}_1, \tag{20}$$

we obtain from (13) the following equation for the function g_a[4]:

$$(u_\xi - \tau)\frac{\partial g_a}{\partial \tau} - \frac{1}{2}\frac{\partial g_a}{\partial u_\xi}\frac{d}{d\tau}\left(\ln \int_{-\infty}^{\infty} g_a\,du_\xi\right) = 0. \tag{21}$$

The boundary condition (18) for the function g_a is rewritten in the form

$$\left.\begin{aligned} &\tau \to -\infty, \quad g_a \to \exp(-\beta u^2) \quad (\beta = T_e/T_i), \\ &\tau \to +\infty, \quad g_a \to 0. \end{aligned}\right\} \tag{22}$$

Equation (21) with boundary condition (22) no longer contains any singularities. The solution of (21), which will be obtained in the next section, describes the distribution of the ions near the edge of the body. It constitutes thus the "rule for circling around" the singularities arising in Eq. (13), and plays a special role in

*We introduce in the definition of the dimensionless ion velocity **u** the electron temperature T_e, bearing in mind that under our conditions $T_e \gtrsim T_i$. In general it is necessary to introduce into this definition the larger of the two quantities, T_e or T_i, since it is precisely the higher temperature which determines the characteristic features of the motion.

*We note that the solution obtained with the boundary conditions (18) is valid only at a sufficiently large distance from the surface of the body, or more accurately when $t \gtrsim b^{-2/3}$. The exact distribution near the surface of the body can be obtained only by using the boundary conditions (16).

the analysis of the character of the perturbation of the plasma in the region close to the body ($t \ll 1$). The boundary condition (18) as $t \to +0$ is rewritten in the form

$$g(\rho, u) = \exp(-\beta u_\eta^2)\, g_a(\tau, -u_\xi), \tag{23}$$

where $\tau = n_1(\rho_0 - \rho)/t$, ρ_0 is the point of the contour of maximum cross section, n_1 is the normal to the contour at the point ρ_0, u_ξ is the velocity in the normal direction, and u_η is the velocity in the tangential direction. The function $g_a(\tau, u_\xi)$ is defined by Eqs. (21) and (22).

The solution of (13) with boundary condition (16) is a universal function of ρ, u, t, and β. Consequently, after going over to dimensional quantities, formula (12) expresses the similarity law in the motion: the pictures of the flow around bodies whose contours are the same in terms of the variables ξ and t are similar. The ratio of the true lengths of the bodies, for example, is equal to the ratio of their velocities.

For not too elongated rapidly moving bodies, the boundary conditions (18) hold true. In this case the pictures of flow around bodies having similar maximal cross sections are similar. For example, if the maximum section of the body is a circle of radius R_0, then, taking into account the cylindrical symmetry of the problem, we obtain from (12) the following expression for the ion distribution function:

$$f = N_0 \left(\frac{M}{2\pi T_i}\right)^{3/2} \exp\left(-\frac{Mv_z^2}{2T_i}\right) g\left(v_1 \sqrt{\frac{M}{2T_e}}, \frac{r_1}{R_0}, \frac{z}{R_0}\sqrt{\frac{2T_e}{Mv_0^2}}; \frac{T_e}{T_i}\right).$$

This formula expresses the similarity rule in this case; the particle density in the perturbed zone can then be represented in the form

$$N(z, \theta) = N_0 f_1\left(\frac{z}{R_0}\operatorname{tg}\theta, \frac{z}{R_0}\sqrt{\frac{2T_e}{Mv_0^2}}; \frac{T_e}{T_i}\right)$$

($\tan\theta = r_1/z$). In particular, at large distances behind the body ($z \gg R_0(Mv_0^2/2T_e)^{1/2}$), the function f_1, as shown in[2] (Sec. 15), takes the form

$$f_1 = 1 - \frac{\pi R_0^2}{z^2}\frac{Mv_0^2}{2T_e} f_2\left(\sqrt{\frac{Mv_0^2}{2T_e}}\operatorname{tg}\theta; \frac{T_e}{T_i}\right).$$

The function f_2 for $T_e/T_i = 1$ was determined in[6,7].

We note that the established similarity laws are similar to those existing in hypersonic aerodynamics[8]. This is not surprising, if we recall the already mentioned dimensional similarity between the corresponding equations.

III. FLOW AROUND A HALF-PLANE

Let us consider the flow around an infinite half-plane. Let the y axis be parallel to the edge of the half-plane, and the ρ axis orthogonal to it. Obviously, the distribution function $g(t, \rho, u)$ does not depend on y:

$$g(t, \rho, u) = g_1(t, \rho, u)\exp(-\beta u_y^2). \tag{24}$$

Recognizing, in addition, that the problem contains no characteristic spatial dimension, we conclude that the function g_1 can depend only on the ratio ρ/t, i.e., the motion is self-similar in this case. The function g_1 consequently coincides identically with the function $g_a(\tau, u_\xi)$ considered in the preceding section ($\tau = \rho/t$, $u_\xi = u$). It is described by the self-similar equation (21) with boundary conditions (22).

Before we proceed to investigate (21) in general form[9], let us consider first two limiting cases corresponding to different values of the temperature ratio $\beta = T_e/T_i$.

1. Assume first that

$$T_i \gg T_e, \qquad \beta \ll 1. \tag{25}$$

In this case, as seen from (10), the potential φ is small and we can neglect the term containing φ in the kinetic equation. Introducing the dimensionless quantities

$$u = \sqrt{\frac{M}{2T_i}}\, v_\rho, \quad \tau = \frac{\rho}{t} = \frac{\rho}{z}\sqrt{\frac{Mv_0^2}{2T_i}}, \quad t = z\sqrt{\frac{2T_i}{Mv_0^2}}$$

(the notation in (12) and (20) is not convenient when $T_e \to 0$; see the footnote preceding Eq. (12)), we obtain the equations and the boundary conditions in the form

$$\left.\begin{aligned} &(u-\tau)\frac{\partial g}{\partial \tau} = 0, \\ &g \to \exp(-u^2), \quad \tau \to -\infty; \quad g \to 0, \quad \tau \to +\infty. \end{aligned}\right\} \tag{26}$$

This means that $\partial g/\partial\tau$ differs from zero only when $u = \tau$. Therefore

$$\frac{\partial g}{\partial \tau} = A(u)\,\delta(u-\tau). \tag{27}$$

Let us integrate this equation with respect to $d\tau$ from $-\infty$ to $+\infty$, and let us use (26). As a result we get

$$A(u) = g|_{\tau\to+\infty} - g|_{\tau\to-\infty} = -\exp(-u^2).$$

If we now integrate (27) with respect to τ from $-\infty$ to τ and use the obtained values A(u), then we get*

$$g(u) = \begin{cases} \exp(-u^2) & \text{if} \quad \tau < u, \\ 0 & \text{if} \quad \tau > u. \end{cases} \tag{28}$$

Accordingly, the particle density is given by the form

$$\frac{N_n(\tau)}{N_0} = \frac{1}{\sqrt{\pi}}\int_\tau^\infty \exp(-u^2)\,du = \frac{1}{2}[1 - \Phi(\tau)], \tag{29}$$

where $\Phi(x)$ is the probability integral. We present also an asymptotic formula for $N_n(\tau)$ as $\tau \to \infty$ (i.e., near the plane itself)

$$\frac{N_n(\tau)}{N_0} = \frac{\exp(-\tau^2)}{2\sqrt{\pi}\tau}, \qquad \tau \gg 1. \tag{30}$$

2. We now consider another limiting case

$$T_i \ll T_e, \qquad \beta \gg 1.$$

In this case the thermal velocity of the ions is smaller than the ordered velocity acquired by them in the electric field. Therefore there is no need to use the kinetic equation. It suffices to write down the equations directly for this translational velocity v. Such an equation has the same form as the hydrodynamics equation, in which the pressure gradient is replaced by the force exerted by the electric field. In the stationary case†

*In this case the motion of the ions is identical to the motion of the neutral particles, since the action of the electric field on the ions is negligibly small when the condition (25) is satisfied. Therefore formula (28) can be readily obtained by starting directly from the geometrical picture of free particle motion.

†We note that the system (31) coincides with the system of equations for the isothermal motion of an ideal gas with temperature T_e.

we have

$$(\mathbf{v}\nabla)\,\mathbf{v} = -\frac{e}{M}\frac{\partial\varphi}{\partial\mathbf{r}} = -\frac{T_e}{M}\frac{\nabla N}{N}, \qquad \operatorname{div}(\mathbf{v}N) = 0. \tag{31}$$

Making the same simplifications as in the derivation of (13), we obtain

$$\left.\begin{aligned} &\frac{\partial\bar{u}}{\partial t} + \bar{u}\frac{\partial\bar{u}}{\partial\rho} + \frac{1}{2N}\frac{\partial N}{\partial\rho} = 0,\\ &\frac{\partial N}{\partial t} + \frac{\partial}{\partial\rho}(\bar{u}N) = 0, \qquad \bar{u} = v_\rho\sqrt{\frac{M}{2T_e}}. \end{aligned}\right\} \tag{32}$$

Finally, changing over to the variable τ, we get

$$\left.\begin{aligned} &(\bar{u}-\tau)\frac{d\bar{u}}{d\tau} + \frac{1}{2N}\frac{dN}{d\tau} = 0,\\ &(\bar{u}-\tau)\frac{dN}{d\tau} + N\frac{d\bar{u}}{d\tau} = 0. \end{aligned}\right\} \tag{33}$$

The system (33) has two solutions: one is trivial, N = const and $\bar{u}$ = const; the other is

$$(\bar{u}-\tau)^2 = \frac{1}{2}, \qquad \bar{u} = \tau + \frac{1}{\sqrt{2}}, \qquad N = C\exp(-\sqrt{2}\,\tau), \tag{34}$$

where C is an arbitrary constant (see[11], p. 443).

The continuous solution satisfying the boundary condition (22) ($N = N_0$, $\bar{u} = 0$ when $\tau \to \infty$) is of the form

$$\bar{u} = 0, \quad N = N_0 \quad \text{if} \quad \tau < -\frac{1}{\sqrt{2}},$$
$$\bar{u} = \tau + \frac{1}{\sqrt{2}}, \quad N = N_0\exp(-\sqrt{2}\,\tau - 1) \quad \text{if} \quad \tau > -\frac{1}{\sqrt{2}}. \tag{35}$$

The electric field produced as a result of the flow is given by

$$E = \frac{v_0\sqrt{MT_e}}{ez\sqrt{2}}F, \qquad F = -\frac{d\ln N}{d\tau} = \begin{cases} 0, & \tau < -\frac{1}{\sqrt{2}},\\ \sqrt{2}, & \tau > -\frac{1}{\sqrt{2}}. \end{cases} \tag{36}$$

The line $\tau = -1/\sqrt{2}$ is a weak-discontinuity line separating the regions of the resting and moving gas. The first derivatives of $\bar{u}$ and N are discontinuous on this line. The discontinuity of the electric field intensity signifies that a screening electric layer exists on this line. Actually, of course, this layer has a finite thickness ~D.[12]

We note that asymptotically, at large values of τ, Eq. (35) leads to much larger values of N than Eq. (30) ($N \sim \exp -\tau\sqrt{2}$) in place of $N_n \sim \exp(-\tau^2)$). This, as will be shown later, is the general result when β is finite, and is connected with the strong influence of the electric field on the ion motion, since some of the ions are accelerated by the electric field. (The same is seen below in Fig. 2b, where the plot for N_n is shown by the dashed line.)

We proceed to an investigation of Eq. (21) in the case of arbitrary values $\beta \sim 1$. Equation (21) is of first order. As is well known, the determination of the function $g_a(u, \tau)$ reduces in this case to a determination of the characteristics of the equation, i.e., of the curves on which the function g_a has a constant value. The equation of the characteristics takes the form

$$\frac{du}{d\tau} = \frac{1}{2}\frac{F(\tau)}{u-\tau}, \tag{37}$$

where

$$F(\tau) = -\beta\frac{d}{d\tau}\left(\ln\int_{-\infty}^{\infty} g_a\,du\right).$$

When $\tau \to -\infty$ we have $F \to 0$ and the characteristics are the straight lines u = const. At each line the distribution function has the value $\exp(-\beta u^2)$. To determine the value of g at the point (u, τ), it is necessary to find the characteristic that passes through this point. The value of g at the point (u, τ) is then equal to $\exp(-\beta u_0^2)$, where u_0 is the ordinate of the line $u = u_0$ reached by the characteristic at $\tau \to -\infty$. Let us investigate qualitatively the course of the characteristics in the (u, τ) plane. First of all, it is obvious that $F > 0$, since the concentration of the plasma decreases with increasing τ. This means that the value of $du/d\tau$ along all the characteristics is larger than zero when $u > \tau$, i.e., the velocity u along the characteristic increases monotonically with increasing τ.

It is very important that none of the characteristics can cross the straight line $u = \tau$. Indeed, near the point $\tau = \tau_0$, in which $u = \tau$, the solution of Eq. (37) is of the form

$$(u-\tau)^2 = F(\tau_0)(\tau-\tau_0).$$

Both branches of this curve are directed towards larger τ. Therefore, taking into account the fact that $u(\tau)$ is monotonic along the characteristics when $u > \tau$, we conclude that the characteristic crossing the line $u = \tau$ cannot belong to the family of characteristics emerging from the region $\tau \to -\infty$, where we certainly have $u > \tau$.

The foregoing investigation shows that in our problem the distribution function g_a is equal to zero when $u < \tau$. Indeed, at large negative τ, the function g_a is Maxwellian and there are no particles with $u < \tau$, owing to the exponential decrease of this function when $u \to \pm\infty$. These characteristics will henceforth not cross the line $u = \tau$, so that no particles with $u < \tau$ will appear. This fact has a simple physical meaning. Indeed, at the initial instant t = 0, all the particles lie outside the half-plane (i.e., at $\rho < 0$). Therefore at the point $\rho/t = \tau$ there can appear particles having a velocity $u > \rho/t$. This is all the more correct if account is taken also of the influence of the electric field, since it only increases the ion velocity u.

We note further that the maximum value of the distribution function at any value of τ is equal to unity. This follows from the fact that at any value of τ there is on the plane (u, τ) a characteristic on which $g_a = 1$. Indeed, the absence of this characteristic at some value of τ would mean that this characteristic, at some finite τ, has turned backwards, which is impossible in view of the monotonic character of $u(\tau)$. This property leads to an important conclusion concerning the asymptotic behavior of $g_a(u, \tau)$ as $\tau \to +\infty$. Indeed, the concentration has an order of magnitude

$$n(\tau) = \frac{N}{N_0} \sim g_{max}\Delta u \sim \Delta u, \tag{38}$$

where Δu is the width of the curve of the distribution function. But as $\tau \to \infty$ we have $n(\tau) \to 0$, and consequently also $\Delta u \to 0$. In other words, with increasing τ the ions become more and more monochromatic, and their temperature decreases. This makes it possible to use directly the hydrodynamic formulas (34) and (35) for the determination of the asymptotic behavior of g_a and n; according to these formulas, the average ion

velocity should be

$$\bar{u}=\tau+\frac{1}{\sqrt{2}}.$$

This means that when $\tau \to +\infty$ all the characteristics should condense near the straight line

$$\bar{u}=\tau+\frac{1}{\sqrt{2}}.$$

Figure 1 illustrates the behavior of the characteristics when $\beta = T_e/T_i = 1$. The asymptotic behavior of the concentration is determined by the formula (34):

$$n=C\exp(-\sqrt{2}\tau), \tag{39}$$

where the constant C should be determined by joining together with the numerical solution. We indicate immediately that when $T_e = T_i (\beta = 1)$ we get $C \approx 0.71$, and when $T_e \gg T_i$, according to (35), we have $C = e^{-1} \approx 0.373$. (The plot of $n(\tau)$ for $\beta = \infty$ is shown dashed in Fig. 2a). To determine $n(\tau)$ for all values of τ, the characteristics were determined numerically[9]. The solution was obtained in steps of τ. The values of $n(\tau)$ and $F(\tau)$ were calculated for each step. The obtained value of F was used to calculate the increment Δu for the next step:

$$\Delta u = u_{k+1} - u_k = \frac{1}{2}\frac{F(\tau_k)}{u_k - \tau_k}\Delta\tau.$$

The obtained values of $n(\tau)$ at different β are shown in Fig. 2. Figure 3 shows plots of the distribution function $g_a(u)$ at different values of τ (for the case $\beta = 1$). It is seen from the figure that in the region of strong rarefaction ($\rho/t = \tau \gg 1$) the ion velocity distribution acquires a needlelike character. The effective ion-velocity spread Δu or the effective ion temperature $T_{i\,eff}$, as seen from (38) and (39), decrease rapidly and exponentially with increasing τ:

$$T_{i\,\mathrm{eff}} \sim (\Delta u)^2 \sim \exp(-2\sqrt{2}\tau). \tag{40}$$

This has a strong influence on the stability of the perturbed zone behind the moving body (see Ch. XI). Plots of the dimensionless force F and of the potential ψ are shown in Fig. 4. Figure 5a shows, in the variables ρ and t, the constant-density surfaces obtained for flow around a half-plane.

The calculations have to be refined in the case of large values of τ. The point is that so far we have assumed $v_z = v_0$ throughout (including in the transition from (31) to (32)) and we have neglected the derivatives with respect to z. It is easy to understand that this approximation is no longer valid when $x \sim z$, i.e., when

$$\tau \geqslant b. \tag{41}$$

Indeed, at such values of τ the potential energy of the ions $e\varphi$ becomes of the order of $Mv_0^2/2$, so that the value of v_z is appreciably altered by the field. On the other hand, the derivatives with respect to z increase with increasing τ and also become appreciable in the region (41). It is important, however, that under the condition (41) we certainly have $\tau \gg 1$. The ions are therefore monochromatic. This makes it possible to use the equations of hydrodynamics (31), which can be rewritten for the dimensionless quantities u and ψ in the form

$$\left.\begin{aligned}(\mathbf{u}\nabla)\,\mathbf{u}+\frac{1}{2}\nabla\psi=0,\\ \operatorname{div}\mathbf{u}+\mathbf{u}\nabla\psi=0,\\ \psi=\ln n,\qquad n=\frac{N}{N_0}.\end{aligned}\right\}$$

These equations can be easily solved in polar coordinates (see[11], Sec. 101). We introduce the azimuthal angle φ, reckoned from the z axis, by means of the relation

$$\operatorname{tg}\varphi=\frac{\tau}{b}=-\frac{\rho}{tb}=\frac{x}{z}.$$

All the quantities will be, as before, functions only of

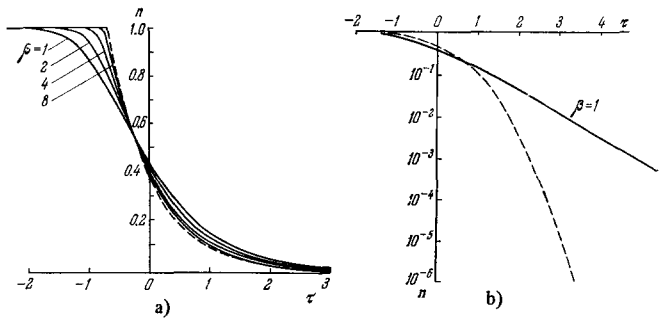

FIG. 2. Flow around a half-plane: a) plot of concentration $n = N/N_0$ against τ; b) the same in a logarithmic scale ($\beta = 1$).

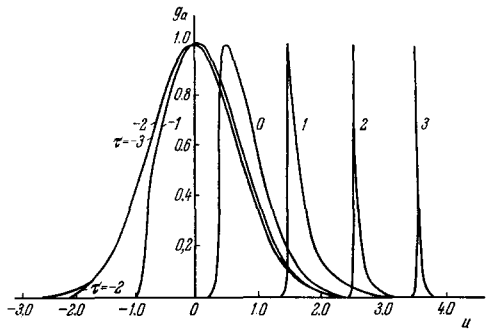

FIG. 3. Flow around a half-plane: distribution function $g_a(u)$ for different values of τ.

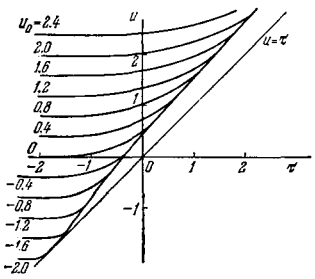

FIG. 1. Flow around a half-plane: behavior of the characteristics in the (u, τ) plane for $\beta = T_e/T_i = 1$.

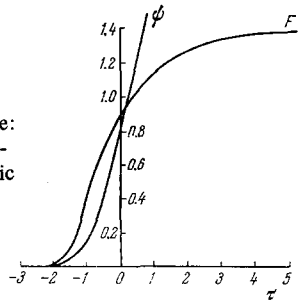

FIG. 4. Flow around a half-plane: dependence of the dimensionless potential $\psi = -e\varphi/T_e$ and of the electric field intensity F on τ.

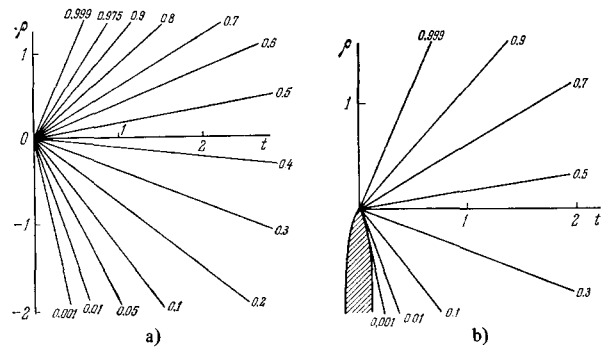

FIG. 5. Surfaces of constant ion density. The values of $n = N/N_0$ are indicated in the figures. a) Flow around a half plane ($\beta = T_e/T_i = 1$); b) flow around a rounded edge of a body ($\beta = 1$, $b = \sqrt{Mv_0^2/2T_e} = 8$).

τ, or, what is the same, of φ.

From the first equation we get a relation indicating the potential character of the velocity u:

$$\frac{du_r}{d\varphi} = u_\varphi,$$

and the Bernoulii equation

$$\psi + u_\varphi^2 + u_r^2 = \psi_0,$$

where ψ_0 is an arbitrary constant.

The continuity equation in terms of the components u_r and u_φ is

$$u_r + \frac{du_\varphi}{d\varphi} + u_\varphi \frac{d\psi}{d\varphi} = 0.$$

Using the foregoing equations, we can reduce the continuity equation to the form

$$\frac{d\psi}{d\varphi}\left(u_\varphi^2 - \frac{1}{2}\right) = 0,$$

whence

$$u_\varphi = \frac{1}{\sqrt{2}}.$$

Further, integrating the equation for u_r, we get

$$u_r = \frac{1}{\sqrt{2}}(\varphi + \varphi_0)$$

(φ_0 is a second arbitrary constant). As a result

$$\ln n = \psi = \psi_0 - \frac{1}{2}(\varphi + \varphi_0)^2 - \frac{1}{2} = \psi_0 - \frac{\varphi_0^2}{2} - \frac{1}{2} - \varphi\varphi_0 - \frac{\varphi^2}{2}.$$

Under the condition

$$\tau \ll b, \quad \varphi \ll 1$$

this expression should go over into (39), from which

$$\varphi_0 = \sqrt{2}\, b, \quad \psi_0 - \frac{\varphi_0^2}{2} - \frac{1}{2} = \ln C(\beta).$$

We finally obtain an expression for the ion density

$$n = C(\beta) \exp\left(-\sqrt{2}\, b\varphi - \frac{\varphi^2}{2}\right). \qquad (42)$$

We note two important features of the obtained formulas. First, near the plane, the longitudinal ion velocity is

$$v_z \approx -\sqrt{\frac{2T_e}{M}}\, u_\varphi = -\sqrt{\frac{T_e}{M}}.$$

The electric field reverses even the sign of the longitudinal velocity. Therefore, ultimately all the ions fall on the back surface of the half-plane. Further, the ion concentration on this surface remains constant and equals

$$n_{\min} = C \exp\left(-\frac{\pi^2}{8} - \frac{\pi b}{\sqrt{2}}\right).$$

Of course, the quasilinear approximation (7) no longer holds at a sufficiently close distance from the edge of the half plane, at large values of b.

IV. FLOW OF A PLASMA CONTAINING AN ION MIXTURE AROUND A HALF PLANE

In an appreciable region of the ionospheric plasma, at altitudes from 400 to 1500 km, there are ions with different masses (mainly oxygen and hydrogen, and to a lesser extent helium[3]). Practical interest therefore attaches to the flow of a plasma containing an ion mixture around a body. The self-similar equation for the problem of flow around a half plane can be readily written out also for this case. Of course, Eq. (21) is now replaced by a system of equations for the distribution functions of each type of ion. For example, in the case of two types of ions with masses M_1 and M_2 we have

$$(u_1 - \tau)\frac{\partial g_1}{\partial \tau} - \frac{1}{2}\frac{\partial g_1}{\partial u_1}\frac{d}{d\tau}\left[\ln\left(\int_{-\infty}^{\infty} g_1\, du_1 + \sqrt{\frac{M_1}{M_2}}\int_{-\infty}^{\infty} g_2\, du_2\right)\right] = 0,$$

$$(u_2 - \tau)\frac{\partial g_2}{\partial \tau} - \frac{M_1}{2M_2}\frac{\partial g_2}{\partial u_2}\frac{d}{d\tau}\left[\ln\left(\int_{-\infty}^{\infty} g_1\, du_1 + \sqrt{\frac{M_1}{M_2}}\int_{-\infty}^{\infty} g_2\, du_2\right)\right] = 0; \qquad (43)$$

here

$$u_1 = v_1/\sqrt{2T_e/M_1}, \quad u_2 = v_2/\sqrt{2T_e/M_1}.$$

The boundary conditions as $\tau \to \infty$ are

$$g_1 \to \exp(-\beta u_1^2), \quad g_2 \to \alpha \exp\left(-\beta u_2^2 \frac{M_1}{M_2}\right).$$

The solution of (43) now depends not only on $\beta = T_e/T_i$, but also on the mass ratio M_1/M_2 and on the ratio of the initial concentrations $\alpha = N_{20}/N_{10}$.

Let us analyze the asymptotic behavior of the solution of large values of τ. To this end, just as in Ch. III, we use the hydrodynamic equations

$$(u_1 - \tau)\frac{\partial N_1}{\partial \tau} + N_1\frac{\partial u_1}{\partial \tau} = 0, \quad (u_1 - \tau)\frac{\partial u_1}{\partial \tau} + \frac{1}{2(N_1 + N_2)}\left(\frac{\partial N_1}{\partial \tau} + \frac{\partial N_2}{\partial \tau}\right) = 0, \qquad (44)$$

$$(u_2 - \tau)\frac{\partial N_2}{\partial \tau} + N_2\frac{\partial u_2}{\partial \tau} = 0, \quad (u_2 - \tau)\frac{\partial u_2}{\partial \tau} + \frac{M_1}{2M_2(N_1 + N_2)}\left(\frac{\partial N_1}{\partial \tau} + \frac{\partial N_2}{\partial \tau}\right) = 0. \qquad (45)$$

We assume for concreteness that $M_2 > M_1$. At large values of τ, there remain in the main the lighter particles, regardless of the ratio of their initial concentrations. Assuming therefore that $N_2 \ll N_1$, we find from (44) that at $\tau \gg 1$ the concentration and the velocity of the light particles are described as before by formulas (34). For heavy particles we obtain from (45)

$$N_2 = C \exp\left(-\sqrt{2}\frac{M_2}{M_1}\tau\right), \quad u_2 = \tau + \sqrt{\frac{M_1}{2M_2}}. \qquad (46)$$

We see therefore that when $M_2 \gg M_1$ the concentration of the heavy ions decreases very sharply with increasing τ. In this case, even for a much larger initial concentration of the heavy particles than of the light

ones, $N_{20} \gg N_{10}$, this concentration decreases with increasing τ in accordance with the self-similar solution (35) only for $N_2 \sim N_1$, i.e., up to

$$\tau_k \sim \frac{1}{\sqrt{2}} \frac{\ln (N_{20}/N_{10})}{\sqrt{M_2/M_1 - 1}}.$$

At larger values of τ, the curve representing the concentration of the heavy particles terminates abruptly, and in practice only the light particles remain. In particular, in the ionosphere, the mass ratio for the hydrogen and oxygen ions is $M_2/M_1 = 16$. In this case the hydrogen concentration near the rear surface of a spherical satellite turns out to be much larger than the oxygen concentration, even if the hydrogen ions amounted to less than 5% in the unperturbed plasma.

We note that the hydrodynamic equations (44) and (45) have an integral

$$N_1 (u_2 - \tau)^2 \left[(u_1 - \tau)^2 - \frac{1}{2} \right] + N_2 (u_1 - \tau)^2 \left[(u_2 - \tau)^2 - \frac{M_1}{2M_2} \right] = 0.$$

It follows from this formula that the location of the weak discontinuity in the hydrodynamic solution is

$$\tau_0 = -\frac{1}{\sqrt{2}} \sqrt{\frac{M_1}{M_2} \frac{N_{20}}{N_0} + \frac{N_{10}}{N_0}}, \quad N_0 = N_{10} + N_{20}.$$

When $\tau < \tau_0$, the plasma is not disturbed. We see therefore that the location of the discontinuity is also shifted very strongly even in the presence of small admixtures of the light gas.

V. FLOW AROUND A WEDGE

So far we have spoken of flow around a half-plane that stands perpendicular to the incoming stream. The results, however, yield immediately the solution for flow around a half-plane with any angle of attack, and for flow around a wedge.

Indeed, let us consider, for example, the region 1 near a wedge ($\rho > 0$) (Fig. 6a). Let the angle between the normal n_1 to the upper face of the wedge and the vector v_0 be α_1. Then the equation of the upper face of the wedge, in terms of the variables ρ and t, takes the form

$$\frac{\rho}{t} = -b \operatorname{ctg} \alpha_1 = \tau_0, \quad b = \sqrt{\frac{Mv_0^2}{2T_e}}.$$

According to (18), the boundary condition on the surface is $g = 0$ when $u < \tau_0$. But this condition is automatically satisfied for the function g_a for all $\tau = \rho/t$. Therefore the distribution of the concentration in the region 1 at $\tau < \tau_0$ is given by the $n(\tau)$ curves shown in Fig. 2. The same pertains also the region 2 ($\rho < 0$) with α_1 replaced by α_2.

In the case of flow around a wedge, interest attaches also to the flux on its surface. The flux on phase 1 is given, as can be readily seen, by the expression

$$j = N_0 v_0 n(\tau_0) \cos \alpha_1 + N_0 \sqrt{\frac{2T_e}{M\pi}}\, j_1(\tau_0) \sin \alpha_1, \qquad (47)$$

where

$$j_1(\tau_0) = \int_{-\infty}^{\infty} u g(u, \tau_0)\, du.$$

A plot of $j_1/\sqrt{\pi}$ at $\beta = 1$ is shown in Fig. 6b, together with the corresponding curve for the neutral gas (dashed line). We see, in particular, that for a half-plane moving parallel to its surface, the electric field at $T_e = T_i$ increases the flux on the surface by a factor of 1.4.* The flux on surface 2 is obtained by replacing α_1 with α_2.

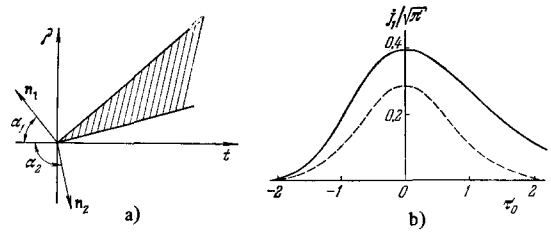

FIG. 6. Flow around a wedge: a) angle scheme; b) ion flux density as a function of τ_0.

VI. FLOW AROUND A ROUNDED EDGE OF A BODY

So far we have investigated flow around a half-plane or a wedge, i.e., around bodies having a sharp edges. In this chapter we consider the perturbation of plasma by a rounded edge of a body[10].

We consider for simplicity the plane problem, i.e., flow around a cylindrical surface with generators parallel to the y axis. The contour of the body in the (ρ, t) plane can be arbitrary. As before, we assume the body to be semi-infinite, i.e., unbounded, for example, in the direction of the axis $\rho < 0$. We note, however, that the results obtained in this case are valid also for a bounded body near its surface, when the particles that have overtaken the second edge of the body are insignificant.

It turns out that the solution of our problem is expressed in terms of the same function $g_a(\tau, u)$ as was obtained in Ch. III. The parameter τ, however, is no longer equal to ρ/t, but is a more complicated function of ρ/t:

$$\tau = \tau(\rho, t).$$

Substituting τ in (13), we get

$$\frac{\partial g}{\partial \tau} \left(\frac{\partial \tau}{\partial t} + u \frac{\partial \tau}{\partial \rho} \right) - \frac{1}{2} \frac{\partial g}{\partial u} \frac{d\psi}{d\tau} \frac{\partial \tau}{\partial \rho} = 0.$$

If we now put

$$u = -u_\xi, \quad \tau = \frac{\partial \tau}{\partial t} \Big/ \frac{\partial \tau}{\partial \rho},$$

then the equation for g will coincide with (21), so that actually we have

$$g = g_a(\tau, -u).$$

On the other hand

$$\tau = \left(\frac{\partial \tau}{\partial t} \right)_\rho \Big/ \left(\frac{\partial \tau}{\partial \rho} \right)_t = -\left(\frac{\partial \rho}{\partial t} \right)_\tau.$$

Integrating this equation, we obtain the sought connection of τ with ρ and t

$$-\rho = \tau t + p(\tau), \qquad (48)$$

*We note that to calculate $j_1(\tau_0)$ there is no need to know the distribution function. Indeed, integrating (21) with respect to du, we obtain $dj_1/d\tau - \tau(dn/d\tau) = 0$, or $j_1(\tau_0) = \int_{-\infty}^{\tau_0} \tau \frac{dn}{d\tau}\, d\tau = \tau_0 n(\tau_0) - \int_{-\infty}^{\tau_0} n(\tau)\, d\tau$.

where $p(\tau)$ is an arbitrary function, which must be determined from the boundary conditions.

Equation (48) defines for each value of τ a straight line on the (ρ, t) plane, on which the distribution function is equal to $g_a(\tau, -u)$. When $p = 0$, all the straight lines intersect at a single point. In this case $\tau = -\rho/t$ and the motion is self-similar, i.e., we return to the formulas of Ch. III. When $p \neq 0$, these straight lines generally do not intersect at one point.

The boundary conditions on the surface of the body, according to (16), are given by

$$g = 0 \quad \text{if} \quad u > \frac{d\rho_0(t)}{dt},$$

where $\rho = \rho_0(t)$ is the equation of the contour of the body in the (ρ, t) plane. The function g_a has the property

$$g_a = 0 \quad \text{if} \quad u_\xi < \tau.$$

Therefore the boundary condition is satisfied if the equality

$$-\frac{d\rho_0}{dt} = \tau$$

is satisfied on the surface, i.e., if

$$-\rho_0(t) = \tau t + p(\tau).$$

The last two equations express in parametric form (with t as the parameter) the function $p(\tau)$ in terms of the equation of the boundary $\rho_0(t)$. Equation (48) then defines the value of τ, and consequently also $g_a(\tau)$, at each point ρ and t.

The foregoing procedure can be very easily effected geometrically. To this end it suffices to draw a tangent on the $t > 0$ side to each point of the contour $\rho_0(t)$ (see Fig. 5b). On these tangents, the distribution function has the values $g_a(\tau, -u)$, where τ is the slope of the tangent to the t axis. Figure 5b shows the lines of constant ion concentration in the case of flow around a circular cylinder ($b = 8$, $\beta = 1$). In this case

$$p(\tau) = -\left[\left(1 + \frac{\tau^2}{b^2}\right)^{1/2} - 1\right].$$

We see therefore that when $t \gg b^{-2/3}$ we have $\tau \approx -\rho/t$. The same result is obtained when the body is replaced by an infinitesimally thin plate. This means that at a sufficiently large distance from the rear surface the exact shape of the body, is immaterial, and only the maximum cross section is of importance (compare Figs. 5a and b). We have thus obtained the same region of applicability of the boundary condition (18) as indicated in the footnote that follows (18).

We note that the solution obtained in this section for the kinetic equation is analogous to the Riemann solution for a simple wave in ordinary hydrodynamics (see, for example,[11], Sec. 94).

VII. FLOW AROUND A PLATE

Let us consider the flow around a plate of width $2R_0$ and of infinite length in the y direction. The plasma flow is perpendicular to the plane of the plate, the thickness of which is assumed to be negligibly small. The distribution of the ions in the perturbed zone behind the plate is described by an equation that follows directly from (13) in the two-dimensional case:

$$\frac{\partial g}{\partial t} + u\frac{\partial g}{\partial \rho} - \frac{1}{2}\frac{\partial g}{\partial \rho}\left(\ln \int_{-\infty}^{\infty} g\, du\right) = 0; \tag{49}$$

Here $g(t, \rho, u)$ is the dimensionless ion distribution function, with

$$u = v_x/\sqrt{2T_e/M},\ \rho = x/R_0,\ t = (z/R_0)\sqrt{2T_e/M}v_0.$$

The z axis is directed, as before, parallel to the velocity of the incoming stream, and the x axis is perpendicular to v_0 and to the axis of the plate.

The boundary conditions for Eq. (49) have the form (23) with $t \to +0$

$$g(t, \rho, u) = g_a\left(\frac{1-\rho}{t}, -u\right) \quad \text{if} \quad \rho \approx 1,$$
$$g(t, \rho, u) = g_a\left(\frac{1+\rho}{t}, u\right) \quad \text{if} \quad \rho \approx -1, \tag{50}$$

where $g_a(\tau, u)$ is the solution considered in Ch. III for the self-similar equation. We note that it is sufficient to consider the problem only for positive values of ρ, since

$$g(t, -\rho, -u) = g(t, \rho, u). \tag{51}$$

The characteristics of Eq. (49) are determined by the conditions

$$\frac{d\rho}{dt} = u,\ \frac{du}{dt} = -\frac{1}{2}\frac{\partial}{\partial \rho}\left(\ln \int g\, du\right). \tag{52}$$

Changing over to a solution of Eq. (49), we take into account the fact that in the region closest to the body (at small values of t), the principal role is played by perturbation by the edges of the body $\rho = 1$ and $\rho = -1$, described by the self-similar solution. It is therefore convenient to write the function g in the form

$$g(t, \rho, u) = g_a\left(\frac{1-\rho}{t}, -u\right) + g_a\left(\frac{1+\rho}{t}, u\right) + g_1(t, \rho, u), \tag{53}$$

where $g_a(\tau, u)$ is the self-similar solution obtained above, and g_1 is a correction function describing the mutual influence of the two fluxes. According to the boundary condition (50), the function $g_1 \to 0$ when $t \to 0$. An analysis presented in[14] shows that the last term in (53) is small, for all values of t, compared with the sum of the first two terms. It is therefore natural to employ the iteration method to solve (49). In other words, we can neglect the function g_1 in the first approximation g^I. We then calculate $\ln \int g^I du$, and substitute it in (52). The characteristic equations (52) are then integrated numerically in steps of t, using the boundary conditions (50). This yields the next iteration g^{II}, etc. In practice it suffices to calculate the second iteration*.

The results of the calculation given in[14] for $\beta = 1$ ($T_e = T_i$) are shown in Fig. 7. The solid curves are the constant ion concentration curves.

The ion distribution function g in the perturbed zone behind the plate is shown in Fig. 8. We see that it

*It is possible to integrate numerically equations (52), without using iterations, by determining $\ln \int g\, du$ from the next step (as was done, for example, in the determination of the self-similar solution). In the case considered here, however, owing to the poor stability of the problem, the solution obtained by this method may acquire increasing oscillations. The increasing oscillations can be suppressed with the aid of special smoothing operations. The solution obtained then coincides with sufficient accuracy with that obtained by iteration [15].

is of the double-hump type. This reflects the fact that two streams coming from different edges of the plate collide.

VIII. FLOW AROUND A CYLINDER

Let us examine the flow around an infinite cylinder of radius R_0. The plasma flux moves in a direction perpendicular to the cylinder axis, with velocity v_0. The ion distribution in the perturbed zone behind the cylinder is described by Eq. (49). As before, relation (51) holds true. We can therefore consider only values $\rho > 0$. The boundary conditions (16) are of the form

$$g(t, \rho, u) = 0$$
$$\text{if} \quad \rho = \sqrt{1 - b^2 t^2}, \; u < 0,$$
$$g(t, \rho, u) = e^{-\beta u^2}$$
$$\text{if} \quad t = 0, \; \rho > 1,$$
$$g(t, \rho, u) = g(t, \rho, -u)$$
$$\text{if} \quad \rho = 0.$$

The last condition follows from the symmetry relation (51).

The characteristic equations are given by (52), as before. They were integrated numerically in steps of t. The results of the calculation[15] are shown in Fig. 9 for $\beta = 1$ ($T_e = T_i$) and $b = 2.50$; the figure shows the constant ion concentration surfaces. Figure 10 shows the distribution of the relative ion concentration on the axis behind a cylinder (curve 2) and behind a plate (curve 1). We see that when $t \gtrsim 1$ the difference between the two pictures is negligible. The same results from a comparison of the constant-concentration surfaces on Figs. 7 and 9. This should be the case, since, as indicated in Ch. II, the exact shape of the body is of little importance for the flow of a plasma stream around the body if the stream velocity is sufficiently large $b \gg 1$ (and at distances not too close to the body). Only the maximum cross section of the body is important. Since the cross sections of the cylinder and of the plate are equal, their flow patterns for $b \gg 1$ are perfectly similar.

Using the results obtained in Ch. VI, we can easily get an analytic expression describing the distribution of the ions in the immediate vicinity of the cylinder at $t \ll 1$. Just as in the case of a plate, for small values of t the distribution function is simply equal to the sum of the distribution functions of the particles that flow around opposite edges of the body (see formula (53)). Let the coordinates of the point under consideration be r and θ in a cylindrical coordinate system in the (ρ, z) plane. We draw from this point tangents to the surface of the cylinder. The angles of inclination of the tangents to the z axis are

$$\varphi_1 = b\left[-\arcsin\left(\frac{R_0}{r}\right) + \theta\right], \quad \varphi_2 = b\left[\arcsin\left(\frac{R_0}{r}\right) + \theta\right].$$

The angle θ is reckoned from the direction of the body velocity v_0. As shown in Ch. VI, the distribution function of the ions flowing around the edge of the body is constant on each tangent and is equal to $f_a(\tau, u)$. The ion concentration is accordingly expressed in terms of the self-similar concentration n_a:

$$n(r, \theta) = n_a(\varphi_1) + K n_a(\varphi_2);$$
$$K = 1 \text{ if } \varphi_1/b \leqslant \pi/2, \quad K = 0 \text{ if } \varphi_1/b > \pi/2.$$

This expression agrees well with the numerical calculation result shown in Fig. 9. In the region near the body, where the concentration n is exponentially small, the formula becomes especially simple

$$n(r, \theta) = C(\beta)\left[\exp\left\{-\sqrt{2}\, b\left[-\arcsin\left(\frac{R_0}{r}\right) + \theta\right]\right.\right.$$
$$\left.\left. - \tfrac{1}{2}\left[-\arcsin\left(\frac{R_0}{r}\right) + \theta\right]^2\right\} + K \exp\left\{-\sqrt{2}\, b\left[\arcsin\left(\frac{R_0}{r}\right) + \theta\right]\right.\right.$$

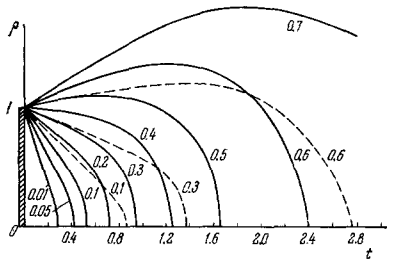

FIG. 7. Constant-concentration surfaces in the case of flow around a plate. The values of $n = N/N_0$ are indicated on the figure ($\beta = 1$).

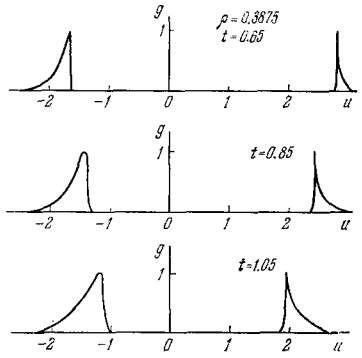

FIG. 8. Ion distribution function g(u) behind the plate ($\beta = 1$).

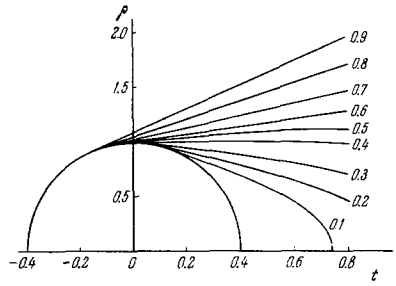

FIG. 9. Constant concentration surfaces in the flow around a cylinder ($\beta = 1$, $b = \sqrt{Mv_0^2/2T_e} = 2.5$). The values of $n = N/N_0$ are indicated on the figure.

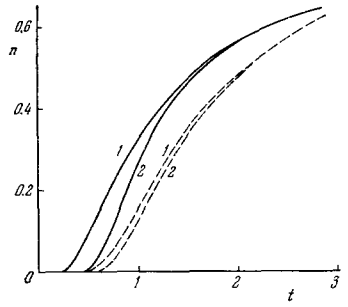

FIG. 10. Plot of $n = N/N_0$ against t at $\beta = 0$ on the axis $\rho = 0$ behind a plate (1) and a cylinder (curve 2, $b = \sqrt{Mv_0^2/2T_e} = 2.5$).

$$-\frac{1}{2}\left[\arcsin\left(\frac{R_0}{r}\right)+\theta\right]^2\Big\}\Big];$$

$K=1$ if $\theta-\arcsin\left(\frac{R_0}{r}\right)\leqslant\frac{\pi}{2}$, $K=0$ if $\theta-\arcsin\left(\frac{R_0}{r}\right)>\frac{\pi}{2}$. (54)

(We have written formula (54) with allowance for the change of the longitudinal velocity of the ions in accordance with (42).)

IX. FLOW AROUND A DISC

We now consider the problem of flow of a plasma flux around a round disc of radius R_0. The plasma moves perpendicular to the plane of the disc. As is clear from the results of Ch. II, this problem is actually of very general significance. Such a disc can be approximately replaced by any body of revolution, if its length R_Z is not too large, $R_Z\sqrt{2Te/Mv_0^2}\ll R_0$. The results obtained for the disc will be valid also for such a body of a sufficiently large distance from it. In particular, the flow around a body of revolution with a flat rear wall reduces to the disc problem.

In view of the axial symmetry of the problem, we shall have to rewrite Eq. (13) in cylindrical coordinates ρ, φ, u_ρ, and u_φ (u_ρ—projection of the velocity $\mathbf{u}$ on the direction of ρ, and u_φ is a projection of $\mathbf{u}$ on the direction perpendicular to ρ).

The distribution function is then practically independent of φ, and in place of u_φ it is necessary to introduce the variable

$$m=u_\varphi\rho,$$

which has the meaning of a dimensionless projection of the angular momentum of the ion on the z axis. m is then an integral of the motion and enters in the equation only as a parameter.

To transform Eq. (13) to the new variables, we note that its form is

$$\frac{dg}{dt}=0,$$

and the derivatives of $\mathbf{u}$ and ρ with respect to t are determined by the Hamilton equations with the Hamiltonian function

$$\mathcal{H}=\frac{\mathbf{u}^2}{2}+\frac{1}{2}\psi(\rho)=\frac{1}{2}\left[u_\rho^2+\frac{m^2}{\rho^2}+\psi(\rho)\right].$$

The corresponding equations for $\dot\rho$ and $\dot u_\rho$ are

$$\frac{d\rho}{dt}=\frac{\partial\mathcal{H}}{\partial u_\rho}=u_\rho,\quad \frac{du_\rho}{dt}=-\frac{\partial\mathcal{H}}{\partial\rho}=\frac{m^2}{\rho^3}-\frac{1}{2}\frac{\partial\psi}{\partial\rho}. \tag{55}$$

Differentiating g and taking (55) into account, we obtain finally the equation in terms of the new variables

$$\frac{\partial g}{\partial t}+u_\rho\frac{\partial g}{\partial\rho}+\left(\frac{m^2}{\rho^3}-\frac{1}{2}\frac{\partial\psi}{\partial\rho}\right)\frac{\partial g}{\partial u_\rho}=0. \tag{56}$$

We note that (55) are the characteristic equations for (56). The potential ψ is determined by the relation

$$\psi=\ln n,\ n(\rho,t)=\frac{\beta}{\pi\rho}\int g\,du_\rho\,dm. \tag{57}$$

The boundary conditions for (56), according to (23), are

$$t\to 0,\ |1-\rho|\ll 1,\ g\to\exp(-\beta m^2)\,g_a\left(\frac{1-\rho}{t},\ -u_\rho\right), \tag{58}$$

where $g_a(\tau, u)$ is the solution of the self-similar equation obtained in Ch. III. When t and $\rho\to\infty$, we get

$$g\to\exp[-\beta(u_\rho^2+u_\varphi^2)]=\exp\left[-\beta\left(u_\rho^2+\frac{m^2}{\rho^2}\right)\right].$$

The solution of (56) for arbitrary values of ρ and t has not yet been obtained. We present here the results for sufficiently small values of t:

$$t=\frac{z}{R_0}\sqrt{\frac{2T_e}{Mv_0^2}}\ll 1. \tag{59}$$

We note that for a rapidly moving body the region (59) turned out to be sufficiently large, and (as seen from the results of Ch. VI), it is precisely in this region that the influence of the electric field on the motion of the ions is appreciable. Under condition (59), the solution can be obtained for all values of ρ. It is necessary, however, to consider separately three regions:

1) $|1-\rho|\ll 1$,
2) $1-\rho\gg t$, $\rho\gg 1$,
3) $\rho\ll\sqrt{t}$.

These three regions overlap under condition (59) (regions 1 and 2 when $1\gg 1-\rho\gg t$, and regions 2 and 3 when $\sqrt{t}\gg\rho\gg t$). Therefore, by obtaining the solution in each region, we solve the problem completely.

In region 1, the solution is expressed, in accordance with (58), in terms of the solution g_a of the self-similar equation. At sufficiently large $\tau=(1-\rho)/t$, the ion velocity distribution function u_ρ becomes monochromatic in accordance with (40). Therefore

$$g=\sqrt{\frac{\pi}{\beta}}\exp(-\beta m^2)\,n\delta(u_\rho-\bar u),$$
$$n=C(\beta)\exp\left(-\sqrt{2}\,\frac{1-\rho}{t}\right),\quad \bar u=-\left(\frac{1-\rho}{t}+\frac{1}{\sqrt{2}}\right); \tag{60}$$

Here the constant $C(\beta)$ is determined by the asumptotic form of the function g_a (see (39)).

In regions 2 and 3, the cylindrical character of the problem comes into play. This becomes manifest in the presence in the kinetic equation (56) of the "centrifugal force" m^2/ρ^3 and of the factor $1/\rho$ in the integral (57) for n. These terms cannot change the δ-like character of the distribution function, but change its dependence on ρ, t, and m. Accordingly, we shall seek in these regions g in the form

$$g=h(t,\rho,m)\,\delta(u_\rho-\bar u(\rho,t,m)) \tag{61}$$

(more accurately speaking, in region 3, owing to the appearance of ions reflected from the "centrifugal potential," the distribution function is the sum of two terms of the type (61)).

Substituting (61) in (56) and integrating with respect to du_ρ, we obtain the "continuity equation" for h

$$\frac{\partial h}{\partial t}+\frac{\partial(h\bar u)}{\partial\rho}=0. \tag{62}$$

Further, we multiply (56) by u_ρ and also integrate. As a result we obtain the second equation

$$\frac{\partial}{\partial t}(h\bar u)+\frac{\partial}{\partial\rho}(h\bar u^2)-\left(\frac{m^2}{\rho^3}-\frac{1}{2}\frac{\partial\psi}{\partial\rho}\right)h=0,$$

or, transforming it with allowance for (62),

$$\frac{\partial\bar u}{\partial t}+\bar u\frac{\partial\bar u}{\partial\rho}+\frac{1}{2}\frac{\partial\psi}{\partial\rho}-\frac{m^2}{\rho^3}=0. \tag{63}$$

The potential φ is connected with h by the formula

$$\psi=\ln n,\quad n=\frac{\beta}{\pi\rho}\int_{-\infty}^{\infty}h\,dm. \tag{64}$$

We now consider the region 2. It is easy to understand that in this region the centrifugal force m^2/ρ^3 is insignificant. This is connected with the fact that the velocity u has an order of magnitude $(1-\rho)/t$ (this will be shown later; see (67)). Therefore the kinetic energy $\bar{u}^2/2$ of the ions is much larger than the centrifugal potential m^2/ρ^2 when $\rho \gg t$. If we neglect the centrifugal energy in (63), then the equations cease to depend on m. Therefore the dependence of g on m will be the same as for the function (60), into which (61) should go over as $\rho \to 1$. In other words,

$$g = \sqrt{\frac{\pi}{\beta}} \exp(-\beta m^2)\, \rho n \delta(u_\rho - \bar{u}) \tag{65}$$

(according to (57) n is the ion concentration). For n we obtain a system of equations which coincides, as it should, with the equation of isothermal hydrodynamics in polar coordinates:

$$\frac{\partial n}{\partial t} + \frac{1}{\rho}\frac{\partial}{\partial \rho}(\rho n \bar{u}) = 0,$$
$$\frac{\partial \bar{u}}{\partial t} + \bar{u}\frac{\partial \bar{u}}{\partial \rho} = -\frac{1}{2n}\frac{\partial n}{\partial \rho}. \tag{66}$$

Representing ln n in the form of a series in powers of t

$$\ln n = \frac{a_{-1}}{t} + a_0 + a_1 t + \ldots$$

and analogously for $\bar{u}$, we can readily verify that, accurate to terms of order t, the solution takes the form

$$n = \frac{C(\beta)}{\rho}\exp\left(-\sqrt{2}\,\frac{1-\rho}{t}\right), \quad \bar{u} = -\left(\frac{1-\rho}{t} + \frac{1}{\sqrt{2}}\right), \tag{67}$$

and differs from (60) only in the factor $1/\rho$ in n. (The constants in the solution are chosen such as to make (67) go over into (60) as $\rho \to 1$.)

We note also that by multiplying the function (58) by $1/\rho$ we obtain a solution that is automatically suitable in both region 1 and region 3. This is perfectly natural, since formula (67) takes into account simply the geometric contraction of the contour of the initial circle when the particles move towards the cylinder axis. On the other hand, by estimating the different terms in Eqs. (66), with allowance for the concrete form of formulas (67), we can verify that the electric field does not influence the motion of the ions in the entire region 2. Therefore the same formulas can be obtained by considering the free motion of the ions and stipulating that the solution go over into the self-similar one on the boundary. In this sense, we can consider regions 2 and 1 jointly.

The solution in region 3, at small values of ρ and t, can be obtained by expanding the sought functions ln h and $\bar{u}$ in series. Leaving out the calculations we present here only the final result

$$\left.\begin{aligned}
&\bar{u}_1 = -\frac{1-\rho}{t} - \frac{1}{\sqrt{2}} + \frac{1}{t}\left(1 - \sqrt{1 - \frac{m^2t^2}{\rho^2}}\right),\\
&h_1 = \frac{\sqrt{\pi}\,C(\beta)}{\sqrt{\beta}}\,\frac{\rho}{\sqrt{\rho^2 - m^2t^2}}\exp\left[-\frac{\sqrt{2}}{t} + \frac{1}{t}\sqrt{2(\rho^2 - m^2t^2)} - m^2\beta\right]\\
&\qquad\qquad \text{if } m^2t^2 < \rho^2,\\
&\bar{u}_2 = \frac{1+\rho}{t} + \frac{1}{\sqrt{2}} - \frac{1}{t}\left(1 - \sqrt{1 - \frac{m^2t^2}{\rho^2}}\right),\\
&h_2 = \frac{\sqrt{\pi}\,C(\beta)}{\sqrt{\beta}}\exp\left[-\frac{\sqrt{2}}{t} - \frac{1}{t}\sqrt{2(\rho^2 - m^2t^2)} - m^2\beta\right]\\
&\qquad\qquad \text{if } m^2t^2 < \rho^2
\end{aligned}\right\} \tag{68}$$

($h_1 = h_2 = 0$ when $m^2t^2 > \rho^2$); here $\bar{u}_1$, h_1 and $\bar{u}_2$, h_2 describe respectively two streams, one of which flows to the center of the disc and the other away from the center. The second stream is produced by the particles moving from the opposite edge of the disc; when $\rho \gg t$, as is clear from formulas (68) directly, the ion concentration in the second stream is exponentially small compared with the concentration in the first stream. Therefore the second stream can be disregarded far from the center of the disc (in regions 1 and 2). The distribution function g is thus the sum of two terms determined by formulas (61) and (68). By integrating it in accordance with (64), we obtain the ion concentration

$$\left.\begin{aligned}
&n = 2\sqrt{\pi\beta}\,C(\beta)\frac{1}{t}\exp(-\sqrt{2}t)\,I(\rho/t),\\
&I(\zeta) = \frac{1}{\pi}\int_0^{\pi}\exp(-\beta\zeta^2\sin^2\theta + \sqrt{2}\,\zeta\cos\theta)\,d\theta.
\end{aligned}\right\} \tag{69}$$

A plot of the function $2\sqrt{\pi\beta}\,I(\zeta)$ for different values of β is shown in Fig. 11. At large values of $\zeta = \rho/t \gg 1/\sqrt{\beta}$ we have

$$I(\zeta) = \frac{1}{2\sqrt{\pi\beta}\,\zeta}\exp(\sqrt{2}\,\zeta)$$

and formula (69) for n coincides with (67). The thermal scatter with respect to m is insignificant when $\rho \gg t$. When $\zeta \ll 1/\sqrt{\beta}$ we have

$$I(\zeta) = 1 - (\beta - 1)\frac{\zeta^2}{2} + \frac{\zeta^4}{8}\left(\frac{3}{2}\beta^2 - \beta + \frac{1}{2}\right). \tag{70}$$

We see therefore that on the axis behind the disc ($\rho \to 0$) the ion concentration assumes a finite value that depends on t and β and is determined by the thermal motion of the ions.

The constant ion concentration surfaces in the near region behind the disc, determined by formulas (60), (67), and (69) are shown in Fig. 12.

From Figs. 11 and 12 and from formulas (69) and (70) we see that when $\beta \leq 1$ the concentration of the ions n increases monotonically with increasing ρ. When $\beta > 1$, condensation occurs near the axis $\rho = 0$; its magnitude increases in proportion to $\sqrt{\beta}$ (when $\beta \gg 1$). The minimum value of $n(\rho)$ at $\beta \gg 1$ is determined by formula (69) (see Fig. 11); in this case $\rho_{min} = t/\sqrt{2}$. Changing over with the aid of (12) to the ordinary variables, we see that the point of minimum concentration moves off the axis $\rho = 0$ at an angle $\theta_{min} = \sqrt{T_e/Mv_0^2}$. In other words, when $\beta \gg 1$, the concentration perturbations are maximal on a cone with aperture $\theta = \theta_{min} = \sqrt{T_e/Mv_0^2}$. This cone is analogous

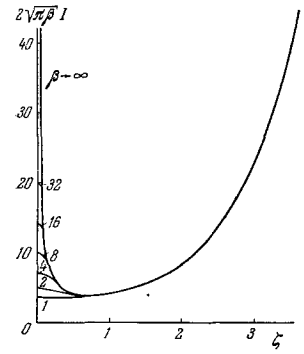

FIG. 11. Flow around a disc: plot of $2\sqrt{\pi\beta}\,I$ against ζ.

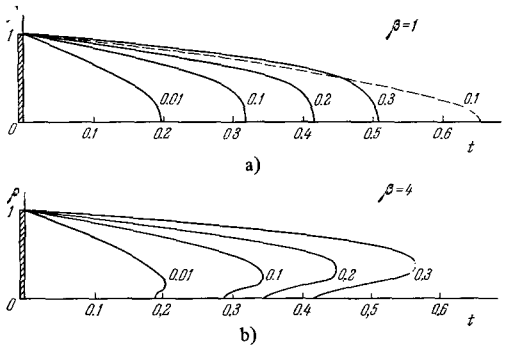

FIG. 12. Constant ion concentration surfaces in flow around a disc. a) $\beta = T_e T_i = 1$; b) $\beta = 4$. The values of $n = N/N_0$ are indicated on the figures.

therefore to the Mach cone in ordinary gas dynamics. An effect of similar type, as shown in[4] takes place at large distances behind a moving body.

It is important, as shown by the calculation, that at small values of $t \ll 1$ the electric field $\partial\psi/\partial\rho$ exerts a strong influence on the motion of the ions only in region 1, which is close to the boundary of the disc: $|1 - \rho| \ll 1$. This is perfectly understandable. Indeed, a finite force cannot influence noticeably the velocity within a short time $t \to 0$, and consequently also the ion concentration. Therefore as $t \to 0$ the electric field can be appreciable only in that region where $\partial\psi/\partial\rho$ is large, i.e., in the region of the singularity near the boundary of the body. But the action of the field in this region has already been taken into account in the self-similar solution on going over from the boundary conditions (18) to the conditions (23). Thus, in calculating the ion distribution function and concentration in the near region behind the body ($t \ll 1$) we can regard the ions as freely moving particles satisfying the condition (23) at $t \to +0$. This makes it possible to find quite easily the ion distribution function when $t \ll 1$ behind a body of arbitrary cross section. Indeed, for freely moving particles is as well known (see[2], Sec. 5),

$$f(t, \rho, \mathbf{u}) = f_0(0, \rho - \mathbf{u}t, \mathbf{u}), \tag{71}$$

where $f_0(0, \rho_0, \mathbf{u})$ is the initial distribution function. It is determined in our case by the boundary condition (23). Using this condition, we obtain from (71)

$$g(t, \rho, \mathbf{u}) = g_a\left(\frac{\mathbf{n}_1(\rho_0 - \rho)}{t}, -u_\xi\right)\exp(-\beta u_\eta^2),$$

where $\rho_0(s)$ is a point on the contour of the body, $\mathbf{n}_1$ is the normal to the contour at the point $\rho_0(s)$, and u_ξ and u_η are the velocity components in the direction normal and tangent to the contour at the point ρ_0. Integrating the distribution function with respect to the velocity $\mathbf{u}$, we can determine the ion concentration. Taking into account the monochromatization of the function g_a(65), we can readily integrate with respect to du_ξ. Changing over, furthermore, from integration with respect to du_η to integration with respect to the length of the contour ds, we obtain in the region behind the body ($\rho_\xi/t > 1$)

$$n(\rho, t) = \frac{C(\beta)\sqrt{\beta}}{\sqrt{\pi}\, t}\oint ds \exp\left(-\sqrt{2}\,\frac{\rho_\xi}{t} - \beta\frac{\rho_\eta^2}{t^2}\right), \tag{72}$$

where ρ_ξ and ρ_η are the components of the vector $\rho_0 - \rho$ along the normal $\mathbf{n}_1$ and the tangent to the contour of the cross section of the body at the point $\rho_0(s)$, and ds is the element of contour length. In particular, if the section of the body is a circle of radius 1, then $\rho_\xi = 1 - \rho\cos\theta$, $\rho_\eta = \rho\sin\theta$, $ds = d\theta$, and formula (72) goes over into (69).

We did not take into account above the variation of the longitudinal component of the ion velocity v_z under the influence of the electric field. As shown in Ch. III, it is significant in the region close to the body. Using formula (42) and repeating the foregoing arguments, we obtain for the concentration behind the disc

$$n(\rho, z) = \frac{\sqrt{\beta}\,C(\beta)}{\sqrt{\pi}}\int_0^{2\pi} d\theta\,\frac{1-\rho\cos\theta}{[z^2+(1-\rho\cos\theta)^2]^{1/2}}\left\{b + \frac{z}{\sqrt{2}(1-\rho\cos\theta)} + \frac{1}{\sqrt{2}}\operatorname{arctg}\left(\frac{1-\rho\cos\theta}{z}\right)\right\}\exp\left\{-\sqrt{2}\,b\operatorname{arctg}\left(\frac{1-\rho\cos\theta}{z}\right) - \frac{1}{2}\operatorname{arctg}^2\left(\frac{1-\rho\cos\theta}{z}\right) - \frac{\beta\rho^2\sin^2\theta\,(1-\rho\cos\theta)^2}{z^2+(1-\rho\cos\theta)^2}\left[b + \frac{z}{\sqrt{2}(1-\rho\cos\theta)} + \frac{1}{\sqrt{2}}\operatorname{arctg}^2\left(\frac{1-\rho\cos\theta}{z}\right)\right]\right\}. \tag{73}$$

This expression coincides with (69) under the condition

$$\left|\frac{1-\rho\cos\theta}{z}\right| \ll 1.$$

On the axis behind the disc ($\rho = 0$) we obtain

$$n(0, z) = \frac{2\sqrt{\pi\beta}\,C(\beta)}{\sqrt{z^2+1}}\left[b + \frac{z}{\sqrt{2}} + \frac{1}{\sqrt{2}}\operatorname{arctg}\left(\frac{1}{z}\right)\right] \times \exp\left[-\sqrt{2}\,b\operatorname{arctg}\left(\frac{1}{z}\right) - \frac{1}{2}\operatorname{arctg}^2\left(\frac{1}{z}\right)\right]. \tag{73a}$$

Near the surface of the disc, formula (73) leads, unlike (69), to finite values of the ion concentration.

X. INFLUENCE OF ELECTRIC FIELD ON THE MOTION OF THE IONS

We have presented above the results of the calculation of the ion distribution in the vicinity of various bodies placed in a supersonic stream of rarefied plasma (half-plane, wedge, plate, cylinder, disc). To understand the influence exerted on the motion of the ions by the electric field, it is necessary to compare these results with a calculation of the concentration of neutral particles, on which the electric field does not act. The expressions describing the distribution of the neutral particles can be readily obtained at an arbitrary form of the surface and velocity of motion of the body (see[2] Ch. II). In[1,2] they were used as approximate expressions for the ion concentration.

Let us consider first the case of a single-temperature plasma $\beta = 1$ ($T_e = T_i$). The concentration of the neutral particles with $T = T_i = T_e$ behind a half-plane is given by expression (29). It is shown by a dashed line in Fig. 2b. It is seen from the figure that at negative or small positive values of $\tau = \rho/t < 0.5$, the distributions of the ions and neutrals are close to each other, and the concentrations differ by not more than 10%. On the other hand, in the region of strong rarefaction, at $\tau \gg 1$, the difference between them is very large. This is clearly seen from Fig. 2b and from a comparison of the asymptotic formulas (30) and (39). Thus, in the case of flow around a half plane, the electric field exerts a decisive influence on the ion distribution in the region of strong rarefaction $N \ll N_0$. On the other hand, in the region where the concentration

of the plasma is appreciable, $N > 0.2N_0$, the influence of the electric field is in general insignificant. A similar conclusion is reached also from a comparison of the distributions of the ions and the neutrals behind a plate or a cylinder; this is also seen from Fig. 7 and 10, in which the dashed curves represent the distribution of the neutral particles. In the region of strong rarefaction behind an axially-symmetrical body (for example behind a sphere or a disc), the difference between the ions and the neutrals is just as large. However, in this case in the zone of not too strong a rarefaction ($N > 0.2N_0$) the deviations of the ion distribution from the neutral-particle distribution are more appreciable (see Fig. 12).

The role of the electric field increases strongly with increasing ratio T_e/T_i. When $T_e \gg T_i$, to obtain similar results, it is actually necessary to consider neutrals with temperature T_e, and this already is a manifestation of a strong influence of the electric field. In addition, when $T_e/T_i \gg 1$, new singularities appear in the ion distribution under the influence of the field; this is seen from Figs. 11 and 12b, namely, the increase of the ion concentration near the axis and the intensification of the perturbation on the Mach cone are due exclusively to the influence of the electric field.

XI. FLOW AROUND STRONGLY ELONGATED BODIES

We consider now the flow around bodies that are strongly elongated in the direction of their motion, i.e., bodies whose longitudinal dimension exceeds the transverse dimension by more than b times.

An example of such a body is a thin plate of width z_0, oriented parallel to the incoming stream. We direct the z axis parallel to the stream, and the x axis perpendicular to the plane of the plate. The dimension of the plate in the y direction is assumed to be infinite. The distribution of the neutral molecules when $b \gg 1$ is given by the formulas

$$n_n = \frac{N_n}{N_0} = \begin{cases} 1, & t \leqslant 0, \\ \frac{1}{2}\left[1+\Phi\left(\frac{\rho}{t}\right)\right], & 0 \leqslant t \leqslant 1, \\ 1-\frac{1}{2}\left[\Phi\left(\frac{\rho}{t-1}\right)-\Phi\left(\frac{\rho}{t}\right)\right], & t \geqslant 1; \end{cases} \qquad (74)$$

here

$$t = \frac{z}{z_0}, \quad \rho = \frac{x}{z_0} b. \qquad (75)$$

Figure 13 shows the constant-concentration contours in the (ρ, t) plane, as determined by formula (74). Figure 14 shows the change of the concentration as a function of ρ for different values of t. It is seen from the figures that the minimum of the concentration is now reached not in the region behind the body, $\rho = 0$, but at an angle $\rho/t \sim 1$. This is seen also from the asymptotic formulas. Indeed, at large distances from the body, $t \gg 1$, the concentration perturbation, according to (55), can be represented in the form

$$\frac{\delta N}{N_0} = \frac{N-N_0}{N_0} = -\frac{1}{\sqrt{\pi}\, t} \frac{\rho}{t} \exp\left[-(\rho/t)^2\right]. \qquad (76)$$

It follows therefore that the maximum of the perturbation is reached on the straight line

$$(\rho/t)_m = 1/\sqrt{2}, \text{ i.e., } x = z\sqrt{T/Mv_0^2}.$$

The influence of the electric field on the motion of the ions in the case of flow around the body when T_i

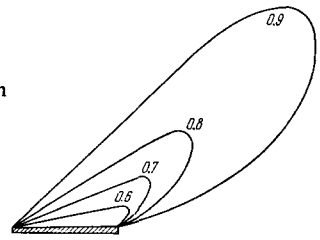

FIG. 13. Constant concentration surfaces in the flow around a plate whose plane is parallel to the incoming stream. The values of $n = N/N_0$ are indicated on the figure.

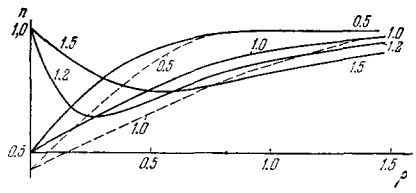

FIG. 14. Flow around a plate whose plane is parallel to the incoming stream: dependence of $n = N/N_0$ on ρ for different values of t indicated in the figure.

$\sim T_e$ is never decisive, since there is no region of high rarefaction here. Therefore the structure of the perturbed region in the vicinity of the body is well described qualitatively by the formulas of the neutral approximation, particularly by formulas (74) for flow around a plate. It is only necessary to replace T by the electron temperature T_e. The dashed lines in Fig. 14 show the results of a calculation of the dependence of n on ρ at $t = 0.5$ and $t = 1$ (when $T_e = T_i$), with account taken of the influence of the electric field. We see that the difference from the neutral curves is not large. The position of the maximum of the perturbation at large distances behind the body, with allowance for the electric field at $T_e = T_i$, is determined by the formula $(\rho/t)_m = 1.4$[13]. When $T_e/T \gg 1$ we have $(\rho/t)_m = 1/\sqrt{2}$, as for a neutral gas.

XII. INSTABILITY OF A PLASMA IN THE WEIGHT OF A BODY

It was shown above that two secondary plasma streams are produced at large distances behind a body in a supersonic plasma stream, and move opposite to each other. The effective temperature of the ions in these streams $T_{i\,eff}$, is exponentially small (see (40) and Figs. 3 and 8); the electron temperature is the same as in an unperturbed plasma. Consequently, $T_e \gg T_{i\,eff}$. We can therefore expect instability in this region, analogous to two-stream instability in a non-equal-temperature plasma[16].

To investigate the stability it is necessary to consider arbitrarily small perturbations of the main solution and to see how they change with time. In the general case such a problem is very complicated. We consider only the most interesting class of perturbations of the fundamental solution. Namely, we take into account the fact that behind the body, in a coordinate system connected with the main plasma stream, two secondary streams moving in the direction of the x axis, which is perpendicular to the velocity of the main stream, collide. It is therefore natural to seek the instability of the plasma against longitudinal waves, which also propagate in the x direction. Since the

perturbed region has a dimension R_0 in the x direction, perturbations with wavelengths larger than R_0 are stable. Let us consider therefore only waves whose length is much smaller than R_0:

$$kR_0 \gg 1. \tag{77}$$

Further, owing to the motion of the main stream, the perturbations produced near the body, i.e., at small values of z, drift with increasing time into the region of large values of z. In other words, the conditions under which the plasma oscillations develop change with time. We consider here only the oscillations whose frequency is sufficiently high, namely $\omega t_0 \gg 1$, where t_0 is the time characterizing the variation of the plasma parameters. Recognizing that the particle concentration changes most rapidly

$$N \sim \exp\left(-\frac{\sqrt{2}}{t}\right) \sim \exp\left(-\frac{R_0 v_0}{z\sqrt{T_e/M}}\right),$$

we find that

$$t_0 = \frac{N}{v_0\left|\frac{\partial N}{\partial z}\right|} \sim \frac{z^2\sqrt{T_e/M}}{R_0 v_0^2}.$$

Consequently, the indicated condition takes the form

$$\frac{\omega z^2\sqrt{T_e/M}}{R_0 v_0^2} \gg 1. \tag{78}$$

If conditions (77) and (78) are satisfied, the plasma can be regarded in the stability analysis as locally homogeneous and quasistationary. In other words, the stability criteria at a given point of the perturbed region and at a given instant of time are the same as in a homogeneous stationary plasma having the same values of the characteristic parameters. It is therefore necessary to investigate first the stability of the homogeneous stationary plasma. To solve this problem, it suffices to consider the dispersion equation and to determine the wave damping coefficient γ. If $\gamma > 0$, then the waves attenuate and the plasma is stable. But if $\gamma < 0$, then small deviations from the equilibrium state increase and the system is unstable. The dispersion equation for ion-acoustic waves in a collisionless plasma, as is well known, are of the form

$$-\frac{4\pi e^2 N}{k^2 T_e} + \frac{4\pi e^2}{kM}\int_C du\,\frac{\partial f_i}{\partial u}\,\frac{1}{\omega - i\gamma + \mathbf{ku}} = 1, \tag{79}$$

where f_i is the ion distribution function in the direction of the velocity u; k, ω, and γ are the wave vector, frequency, and damping coefficient of the considered waves, while C is the integration contour in the complex plane of the variable u, indicated by Landau[17]. In the case of interest to us, the ions constitute two streams with different densities and different effective temperatures. Assuming for simplicity the ion distribution to be Maxwellian in each stream, we get in lieu of (79) the following dispersion equation:

$$(kD_2)^2 + \frac{T_2}{T_e}\left(\frac{N_1}{N_2}+1\right) + 1 - J\left(\frac{\omega - kv_2 - i\gamma}{kv_{T2}}\right) - \frac{T_2 N_1}{T_1 N_2}\left[1 - J\left(\frac{\omega - kv_1 - i\gamma}{kv_{T2}}\right)\right] = 0; \tag{80}$$

Here $D_2 = (T_2/4\pi e^2 N_2)^{1/2}$ is the Debye radius for the second stream; N_1, v_1, vT_1, and T_1 are the concentration, translational and thermal velocities ($zT_1 = \sqrt{T_1/M}$), and the temperature in one stream of ions, and A_2, v_2, vT_2, and T_2 are the same quantities in the second stream; finally, J(z) is a function of the complex variable z, defined by the relation

$$J(z) = z\exp(-z^2/2)\int_{i\infty}^{z}\exp(\tau^2/2)\,d\tau = -i\sqrt{\frac{\pi}{2}}\,z\Phi(z/\sqrt{2}),$$

where $\Phi(z)$ is the probability integral, tables of which are given in[18].

The boundary of the instability region is determined, naturally, by the condition

$$\gamma = 0. \tag{81}$$

When condition (81) is satisfied, the functions J enter in (80) only as functions of a real argument. In this case

$$J(a) = ae^{-a^2/2}\int_0^a \exp(\tau^2/2)\,d\tau - i\sqrt{\frac{\pi}{2}}\,a\exp(-a^2/2) = F_1(a) - iF_2(a). \tag{82}$$

Substituting the expression (82) in Eq. (80) at $\gamma = 0$, we have

$$1 - F_1\left(\frac{\omega - kv_2}{v_{T2}}\right) + \frac{T_2 N_1}{T_1 N_2}\left[1 - F_1\left(\frac{\omega - kv_1}{kv_{T1}}\right)\right] - \frac{T_2}{T_e}\left(\frac{N_1}{N_2}+1\right) + (kD_2)^2 = 0, \tag{83}$$

$$F_2\left(\frac{\omega - kv_2}{kv_{T2}}\right) + \frac{T_2 N_1}{T_1 N_2}F_2\left(\frac{\omega - kv_1}{kv_{T1}}\right) = 0. \tag{84}$$

Since all the parameters which enter here depend only on ρ and t, one of the equations (83) and (84) determines the phase velocity of the wave $\omega/k = v_{ph}(\rho, t)$, and the second establishes the connection between the values of ρ and t, at which $\gamma = 0$, i.e., it determines the boundary of the instability region.

Let us consider the region behind the plate; near the plate we have $\rho < 1$ and $t \lesssim 1$; for concreteness we assume that $\rho \geq 0$ and that the quantities N_1, v_1, and T_1 characterize the stream flowing from the boundary $\rho = 1$, while N_2, v_2, and T_2 characterize the stream from the opposite boundary $\rho = -1$. We consider first Eq. (84). We take into account the fact that the ion temperatures T_1 and T_2 are exponentially small (compared with T_e) when $t \ll 1$, and the velocities v_1 and v_2 are larger than $\sqrt{T_e/M}$. Consequently, the ratios v_2/vT_2 and v_1/vT_1 are exponentially large quantities, and $v_2/vT_2 \gg v_1/vT_1$ everywhere except at the point $\rho = 0$, since $T_2 \ll T_1$. It is then natural to seek the solution of (84) in the form

$$\omega = kv_2(1+\Delta), \tag{85}$$

where $\Delta \ll 1$. Substituting (85) in (84), we get

$$\Delta = \sqrt{\frac{MT_2}{T_e T_1}}(v_1 + v_2) = \sqrt{\frac{2T_2}{T_1}}(u_1 + u_2), \tag{86}$$

where $u_1 = v_1/\sqrt{2T_e/M}$ and $u_2 = v_2\sqrt{2T_e/M}$ are the dimensionless velocities (they are defined by formulas (34)). Substituting now expressions (85) and (86) in (83), and putting $kD \to 0$ in (83), we arrive at the relation

$$2\left(1 + \frac{N_1}{N_2}\right)(u_1 + u_2)^2 = \frac{T_1}{T_2}. \tag{87}$$

For the values of ρ and t satisfying relation (87), the damping coefficient of the ion-acoustic waves is $\gamma = 0$. Relation (87) thus determines the boundary of the stability region of the plasma behind the plate; it is shown in Fig. 15; the plasma region above the curve of

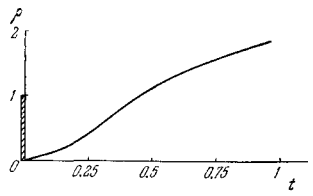

FIG. 15. Boundary of the stability region in the case of flow around a plate ($\beta = 1$).

Fig. 15 is unstable*.

Figure 15 shows the results for a single-temperature plasma. With increasing ratio T_e/T_i, the instability region broadens and its increments increase. We note also that we have considered here instability behind the plate. The role of the instability weakens with increasing effective length of the body (in terms of the variables ρ and t).

XIII. POTENTIAL OF THE SURFACE OF THE BODY

Flow of plasma around the body was considered above under the assumption that the surface of the body has an appreciable negative potential. Such a potential is actually established on a body in the absence of a magnetic field and in the absence of electron emission. In fact, thermal electrons usually are absorbed upon collision with the surface of the body, and the ions become neutralized[5]. The ion and electron fluxes incident on the surface of the body should be therefore equal. But if the body moves with velocity $v_0 \ll \sqrt{T_e/m}$, then the flux of ions to an uncharged body is smaller than the flux of electrons. The surface of the body therefore acquires an appreciable negative charge, which reflects the greater part of the electrons.

In the presence of electron emission from the surface of the body, the potential increases and can reverse sign. Under real conditions of the ionosphere and magnetosphere, the emission can be produced by the photoeffect[19-21], by surface heating[22], by the action of corpuscular streams[21-23]; artificial emission of fast or thermal electrons is also possible.

When a conducting body moves in a magnetic field, an important role can be played by polarization resulting from the action of the Lorentz force. In this case, a certain inhomogeneous distribution of the potential is established on the surface of the moving body. This was first pointed out by D. Beard and F. Johnson[20]. It was subsequently investigated also theoretically and experimentally under laboratory conditions[24,25], and in the ionosphere[34,52]. We shall consider this question here in greater detail.

Let a spherical body of radius R_0 move with velocity v_0 in a direction perpendicular to the magnetic field H. We assume, as usual, that $R_0 \gg D$ and $b = (Mv_0^2/2T_g)^{1/2} \gg 1$ (D—Debye radius). We determine the distribution of the electric-field potential φ on the surface of the conducting body. In the coordinate system moving with the body, we direct the z axis along - v_0 and the x axis along H. Then

$$\varphi = \varphi_0 + \frac{v_0}{c} Hy = \frac{v_0}{c} H(y - y_0). \tag{88}$$

*The ion distribution function was assumed in the calculation to be equal to the sum of two self-similar solutions (formula (53) with $g_1 = 0$).

The constant $y_0 = -c\varphi_0/v_0H$ is determined from the condition for the equality of the total fluxes of the electrons and ions to the body. It is assumed, as usual, that the electrons are absorbed by the surface and that the ions recombine completely on the surface). At not too large body dimensions $R_0 \lesssim v_0/\Omega_{Hi}$, the ion flux does not depend on the surface potential:

$$J_i = N_0 v_0 \pi R_0^2. \tag{89}$$

Neglecting the action on the electrons by the electric field that penetrates into the interior of the plasma, the electron flux density is

$$j = \begin{cases} j_0 \exp(e\varphi/T_e) & \text{if} \quad \varphi \leqslant 0, \\ j_0 & \text{if} \quad \varphi > 0; \end{cases} \tag{90}$$

Here $j_0 = N_0\sqrt{T_e/2\pi m}$ is the density of the electron heat flux on the charged surface (see[2], p. 356). The total electron flux is

$$J_e = \int j\, ds = 2\int_{-R_0}^{R_0} \sqrt{R_0^2 - y^2}\, j(y)\, dy. \tag{91}$$

In the last expression we took into account the fact that the electron flux, according to (88) and (90), depends only on y and that the electrons, as well as the ions, fall only on the frontal surface of the body (by virtue of the condition $b \gg 1$[1,2]). Substituting now expressions (90) in (91), we get

$$J_e = 2R_0^2 j_0 \left[P\left(\alpha, \frac{y_0}{R_0}\right) + \frac{\pi}{4} - \frac{1}{2}\arcsin\left(\frac{y_0}{R_0}\right) - \frac{1}{2}\frac{y_0}{R_0}\sqrt{1 - \frac{y_0^2}{R_0^2}}\right],$$

$$P\left(\alpha, \frac{y_0}{R_0}\right) = \int_{1-(y_0/R_0)}^{2} \sqrt{x(2-x)}\exp(-\alpha x)\, dx; \tag{92}$$

here α is a characteristic dimensionless parameter:

$$\alpha = \frac{ev_0 H R_0}{cT_e}. \tag{93}$$

We determine y_0 by equating the total fluxes of the electrons (92) and of the ions (89). Naturally, a region with a positive potential exists on the body only if $y_0 < R_0$. The radius of the body R_{0c} at which a positive potential first appears is determined by the condition $y_0 = R_{0c}$. From (92) and (89) we obtain in this case

$$\pi\sqrt{\frac{\pi}{2}}\left(\frac{mv_0^2}{T_e}\right)^{1/2} = \int_0^2 \sqrt{x(2-x)}\exp(-\alpha x)\, dx. \tag{94}$$

We take into account the fact that the quantity on the left is small. The equality (94) can therefore hold only if $\alpha \gg 1$. Then, changing over under the integral sign to a new variable $\tau = \alpha x$, we can replace the upper limit of integration with respect to τ by ∞. Accurate to small terms (of the order of $1/4\alpha$), the integral is equal to $\pi^{1/2}/2^{1/2}\alpha^{3/2}$. Consequently

$$R_{0c} = \frac{cT_e^{4/3}}{\pi^{2/3} m^{1/2} v_0^{5/3} eH}. \tag{95}$$

Under the conditions of the ionosphere we have $R_{0c} \sim 0.5$–5 meters.

At large values of $R_0 \gg R_{0c}$, the term $P(\alpha, y_0/R_0)$ in expression (92) is insignificant. We then obtain for y_0

$$y_0 = R_0\left[1 - \frac{3^{2/3}\pi}{2}\left(\frac{mv_0^2}{T_e}\right)^{1/3}\right].$$

Thus, when $R_0 \gg R_{0c}$, a part of the body, with coordinates $y_0 \leq y \leq R_0$ is at a positive potential relative to

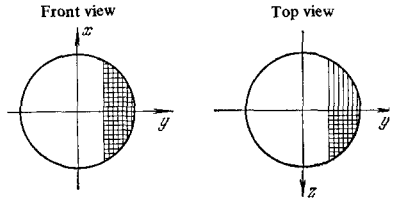

FIG. 16. Potential on the surface of a sphere moving in a magnetic field.

the plasma. This region is shown shaded in Fig. 16. The double shading designates the region on which the electrons are mainly absorbed. When $R_0 \gg v_0/\Omega_{Hi}$, the ions fall on the entire frontal surface, and when $R_0 \ll v_0/\Omega_{Hi}$ they fall only on the unshaded region.

A similar calculation for a cylinder with axis perpendicular to the magnetic field, moving with velocity v_0 in a direction perpendicular to the axis and to H, yields

$$L_{0c} = \frac{cT_e^{3/2}}{\sqrt{2\pi} m^{1/2} e v_0^2 H};$$

Here L_{0C} is the length of the cylinder at which positive potential appears on the edge of the body. When $L \gg L_{0C}$, the fraction of the cylinder length L on which the potential is positive amounts to pL, where

$$p = \frac{N_0 v_0}{j_0} = \sqrt{\frac{2\pi m v_0^2}{T_e}}.$$

We see therefore that polarization produces a region of positive potentials on large bodies moving in a magnetic field. This results in interesting singularities when plasma flows around such bodies. Indeed, in the case when there is an appreciable negative potential on the surface of the body, the body interacts mainly with the plasma ions. This was precisely the case considered above (see also[1,2]). The concentration of the electrons in the vicinity of the body is altered only to the extent that the ion concentration is perturbed. The ions move more slowly than the body. A strongly elongated wake is produced in the plasma and expands slowly with increasing distance from the body.

One can expect the picture of the perturbation produced by the regions of positive potential to be essentially different. Indeed, the plasma electrons move along the force lines of the magnetic field much more rapidly than the body. All are absorbed in the surface regions that are at a positive potential. Therefore perturbed zones, from which electrons are depleted, should therefore extend from these regions along the magnetic-field force lines. This produces an electric field that creates an appropriate perturbation also among the ions. The dimension of the perturbed zone in the direction of the magnetic-field force lines is larger by a factor v_{Te}/v_0 than the dimension of the body (v_{Te}—thermal velocity of the electrons). Thus, flow around a large body with $R_0 > R_{0C}$ should produce, besides the usual wake behind the main negatively-charged part of the body, also thin "wings" extending from the positively charged part of the body along H and differing in structure from the main weight. The effect becomes more intense for bodies that emit electrons.

XIV. NUMERICAL CALCULATIONS WITH ALLOWANCE FOR THE FINITE DEBYE RADIUS

We have previously started from the equation of quasineutrality of the plasma (7), which replaced the Poisson equation. Such an approximation corresponds to the limit $R_0/D \to \infty$, i.e., it is valid under conditions when the characteristic dimension of the perturbed region is large compared with the Debye radius. In many problems, however, this approximation is insufficient.

First of all, the quasineutrality approximation is not valid if the dimension of the body is smaller than or of the order of the Debye radius.

Further, a finite Debye radius is essential in the analysis of the double-layer adjacent to the surface of the body, where the quasineutrality is violated. The dimension of this layer increases behind the body, where the particle concentration is small. It increases also when the potential of the body increases. Particularly important are effects connected with the deviation from quasineutrality in the case when the potential of the body is very high:

$$|\varphi_0| \gg \frac{T_e}{e}\left(\frac{R_0}{D}\right)^{4/3}.$$

In this case the double layer may become commensurate in size with the body.

An investigation of all these cases requires in fact a solution of the Poisson equation. A thin double layer at the surface of the body can be calculated analytically. The corresponding results are reported in[2], Sec. 14, and in[26]. In the remaining cases it is necessary to integrate Poisson's equation numerically. Recently, much attention has been paid to such calculations. We shall describe briefly some of the relevant papers, confining ourselves mainly to the formulation of the problem and to the results. The description of the numerical procedure is beyond the scope of the present review.

1. Flow of a Stream of Cold Ions Around a Body with Dimensions on the Order of the Debye Radius

M. V. Maslennikov and Yu. S. Sigov[27] performed a simultaneous numerical integration of the ion equations of motion and the Poisson equation. The correct solution of such a problem entails great difficulties, connected with the poor stability of the Poisson equation. These difficulties were overcome in[27] with the aid of a special calculation procedure, and reliable results were obtained. The electrons were assumed to have a Boltzmann distribution, and the thermal motion of the ions was neglected ($T_i = 0$). The results of the calculations—the surfaces of constant values of the potential $\psi = e\varphi/T_e$ at $R_0 = D$ and of the surface potential $\varphi_0 = 0$ are shown in Fig. 17. Attention is called to the oscillating dependence of the potential on the distance. It can be assumed that the presence of such oscillations is due to the neglect of the thermal motion of the ions: in the absence of thermal motion, the ion-acoustic waves propagate without Landau damping, and this contributes to the appearance of the oscillations. When $T_i \sim T_e$, the thermal motion should lead to a smearing out of the oscillations.

2. Iteration Solution of the Problem of Flow Around a Plate with Dimensions on the Order of the Debye Radius

J. Taylor[28] developed an iteration procedure for a simultaneous solution of the Poisson equation and the kinetic equation. As the zeroth approximation he chose the ion distribution function in the absence of an electric field. Therefore the iterations are carried out with respect to the electric field. It should be emphasized that, by the same token, account is taken of the thermal motion of the ions, and the model under consideration is perfectly realistic. On the other hand, as seen from the discussion presented at the end of Ch. IX, the distribution of the neutral particles is a good approximation for the distribution of the ions only in a region of not too large a rarefaction. Consequently, the iteration converges poorly near the body. Figure 18 shows a plot of $n = N/N_0$ against $\rho = x/R_0$ at fixed $\xi = z/R_0$. The body is a plate of thickness 0.6D (in the direction of the z axis) and of width $2R_0 = 3D$ (in the direction of the x axis). The Mach number is $b = 6$ and the potential of the body is $e\varphi_0/T_e = -2.75$. The figure shows the zeroth approximation (dashed lines) and the first approximation (solid lines). In the case of a high potential on the body ($e\varphi_0/T_b = -14$), the plot of N/N_0 against ρ becomes nonmonotonic, which agrees qualitatively with the results of[27] for cold ions.

3. Flow Around a Strongly Charged Body

The problem of flow around a body charged to such a degree that $|e\varphi_0| \gg Mv_0^2$, was solved by E. Walker[29], who did not consider a body of any concrete shape. Instead, it was assumed in fact that all the particles crossing a certain limiting equipotential surface are drawn in by the field and are absorbed by the body. The physical basis for such an approximation lies in the fact that at very high potentials the dimension of the region in which the quasineutrality is violated and strong fields exist becomes much larger than the dimension of the body*. In this case the concrete shape of the body can be irrelevant.

The problem was solved numerically by simultaneously solving the Poisson equation and the equations of motion of the ions. Among the shortcomings of the calculation are the use by the author of a poorly justified condition for the potential on the unperturbed plasma boundary, and the arbitrary choice of this boundary itself. We shall not discuss this question in detail.

Figure 19 shows the surfaces of constant ion concentration $n_+ = N_i/N_0$ calculated in[29]. They were plotted for $b = 5.8$. The figure shows also the equipotential surface for

$$\psi = \frac{2e\varphi_0}{Mv_0^2} = -40.$$

On the boundary of the unperturbed plasma (hemisphere, $\rho = 20$), ψ is assumed equal to -0.001. The unit length in the figures is

$$D_0 = D\sqrt{b} = \sqrt{\frac{Mv_0^2}{8\pi N_0 e^2}}.$$

Figure 19 was plotted for cold ions, and Fig. 19b for an equal-temperature plasma. It is seen from the figures that in this case of very strong potential on the front and on the sides of the body, the thermal motion

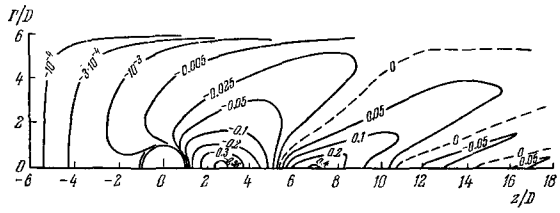

FIG. 17. Constant-potential surface in flow around a sphere of radius $R_0 = D$. The values of $\psi = e\varphi/T_e$ are indicated on the figure.

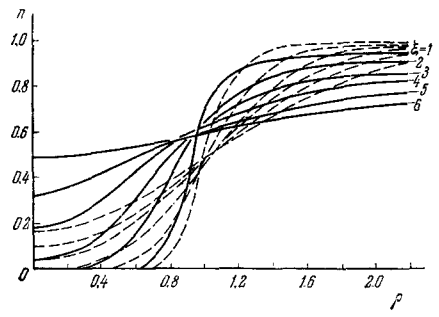

FIG. 18. Dependence of the concentration $n = N/N_0$ on $\rho = x/R_0$ in flow around a plate.

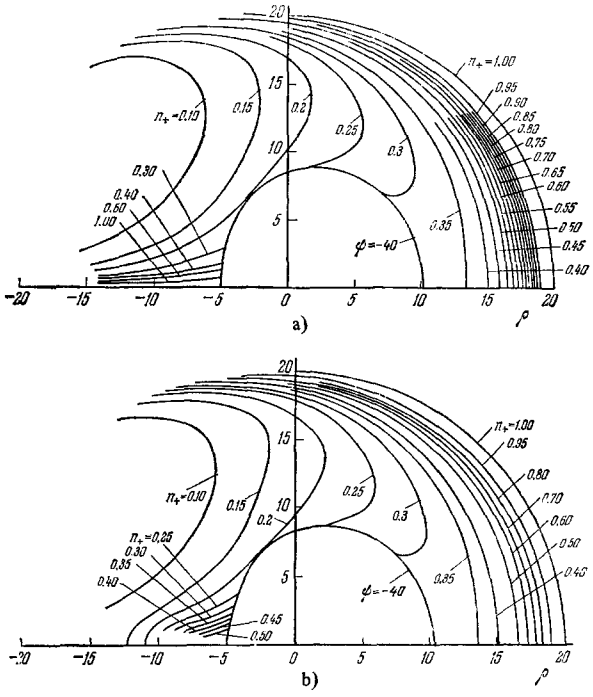

FIG. 19. Surfaces of constant ion concentration $n_+ = N_i/N_0$ in the vicinity of a strongly charged body. a) $\beta = T_e/T_i = \infty$; b) $\beta = 1$.

*The problem was solved by an analogous method for a strongly charged body at rest by J. Langmuir and K. Blodgett [30] (see also [2], Sec. 39). As follows from that paper, the dimension of a region strongly perturbed by the field is much larger than the radius of the body R_0, provided $|\varphi_0| \gg (T_e/e)(R_0/D)^{4/3}$.

of the ions is of no importance. To the contrary, behind the body, (near the z axis), the difference between the curves of Figs. 19a and 19b is large even qualitatively.

4. Flow Around Bodies of Small Dimensions

A. M. Moskalenko and V. S. Knyazyuk[31,32] have considered the flow around spherical bodies, the radius of which is much smaller than the Debye radius in the unperturbed plasma. In this case, the electric field in the vicinity of the body is of the Coulomb type. If, in addition, the surface potential φ_0 is not too large:

$$|\varphi_0| \ll \frac{T_e}{e}\frac{D}{R_0}, \quad D \gg R_0, \tag{96}$$

in the region $r > D$ (where the Coulomb field is distorted as a result of the Debye screening) the electric field is weak ($\varphi \sim \varphi_0(R_0/r) \ll T/e$) and has little influence on the motion of the particles. The exact form of the field when $r > D$ is therefore irrelevant. Thus, when conditions (96) are satisfied, and perturbations are considered in the vicinity of the body at $r < D$, a Coulomb electric field can be assumed. This greatly simplifies the calculation and makes it possible to obtain an expression in terms of quadratures for the concentration and fluxes of the particles in the vicinity of the body.

The result of a numerical tabulation of the distribution of the ions is shown in Fig. 20. In Fig. 20a ($\varphi_0 = -T/e$, $v_0 = \sqrt{2T/M}$) are shown the surfaces of constant values of the ion density (the numbers on the curves give the values $n = N_i/N_0$). The dashed curve shows the distribution of the ions in the vicinity of the body at rest, for the same surface potential. We see that the unperturbed part in front of the moving body is closer to its surface. Behind the body, near the surface, there is a small rarefaction zone, followed by a region of increased concentration. The maximum of the ion concentration is reached on the axis behind the body at a certain distance (on the order of $2.5R_0$) from its surface. The increase of the ion concentration in this region is a consequence of the gathering action of the electric field. Qualitatively these results are similar to those obtained by Walker[29].

Figure 20b shows the distribution of the ions behind the body, obtained neglecting their thermal motion. The surface potential is $\varphi_0 = -Mv_0^2/2e$. The solid curves are surfaces of equal ion concentration. The dashed curve separates the regions into which the ions fall after moving around the body from the other side, from the region in which they fall and are absorbed on the surface of the body. In the region where such ions fall, the concentration is higher. This results in a discontinuity in the ion-concentration distribution. Near the body there is a region with zero ion concentration (it is delineated in the figure by a thin solid line). When thermal motion is taken into account, the discontinuity line becomes smeared out.

In[31,32], they also found the distribution of the particle flux on the surface of the body. With increasing surface potential, the distribution of the particle flux over the surface becomes more and more symmetrical. It is interesting that at large values of φ_0 the total ion flux on the surface of a moving body decreasing with increasing body velocity.

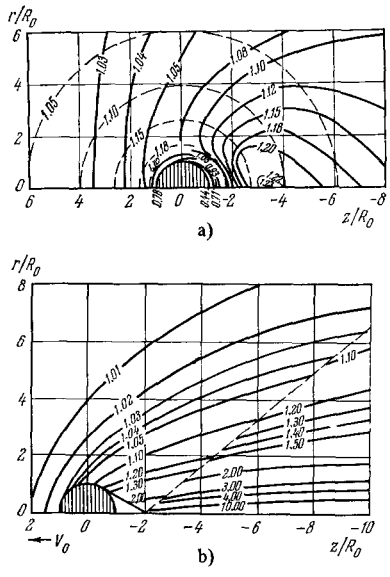

FIG. 20. Surfaces of constant ion concentration $n_+ = N_i/N_0$ in the vicinity of a small body with $R_0 \ll D$.

5. Flux of Ions on the Surface of a Moving Plate

We have determined above the flux of ions on a plate, when the width of the plate z_0 is much larger than the Debye radius, $z_0 \gg D$. In this case, at not too high field potentials on the surface of the plate φ_0, the flux density does not depend on φ_0 and is determined by expression (47) given in Ch. V. It is important, however, that at large values of $b \gg 1$ the flux density decreases strongly with increasing angle between the normal to the plate end and the velocity direction v_0. At angles close to $\pi/2$, the flux can be strongly influenced by the presence of a charged double layer even at not too high potentials φ_0.

A calculation of the flux (with allowance for the double layer) for the case when the thickness of the double layer is smaller than the width of the plate, neglecting thermal motion of the ions, is presented in[14]. It is shown there that the ion flux on the surface of the plate, I_i, as a function of the angle θ between n and v_0, is described by the formula

$$\frac{I_i}{N_0 v_0 S} = \cos\theta + \frac{2\sin\theta}{3}\frac{DN_0^{1/2} j(\tau)}{z_0 v_0 N_a^{3/2}(\tau)}\left[\left(1 + \frac{2e|\varphi_0| N_a^2(\tau)}{Mj^2(\tau)}\right)^{1/2} - 1\right]^{3/2}, \quad \tau = -b\operatorname{ctg}\theta. \tag{97}$$

The concentration $N_a(\tau)$ has been determined in Ch. III, and the flux $j(\tau)$ is given by formula (47) for $\alpha_1 = \theta$. The second term in (97) gives that part of the flux which is connected with the finite thickness of the double layer. We see that at large values of θ, the role of this term becomes appreciable and even decisive. The result of the calculation of the dependence of I/I_0 on θ for $b = 2.5$, $z_0/D = 17.7$, and $-e\varphi_0/Te = 35$ is shown in Fig. 22. The dashed curve in the figure gives the flux density without allowance for the influence of the electric field of the double layer.

6. Flow of Single-temperature Plasma Around a Sphere

After the present review was completed, we learned of an interesting paper[38] in which a simultaneous numerical solution was obtained for the equations of

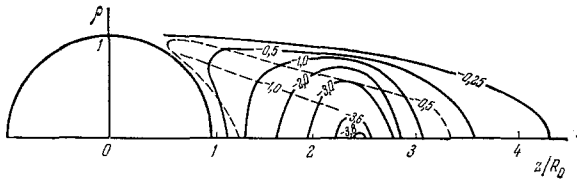

FIG. 21. Surfaces of constant potential behind a sphere of radius $R_0 = 50D$.

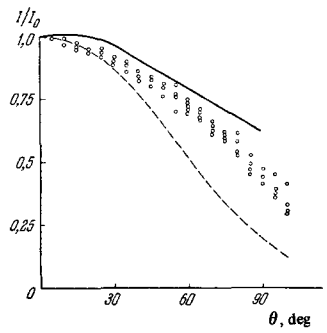

FIG. 22. Ion flux on a flat probe as a function of the angle θ between the normal to the surface of the probe and the direction of probe motion.

motion of the ions and for the Poisson equation, for the case $T_e = T_i$. The solution was performed by iteration, and the zeroth approximation was taken to be the potential distribution obtained in[1], neglecting the influence of the electric field on the motion of the ions. The results of the calculation for a sphere (with, apparently, $R_0/D = 50$) show that deviations from quasineutrality have little effect on the ion distribution, but lead, as they should, to a noticeable change in the potential distribution at $z \sim R_0$. The obtained equipotential surfaces are shown in Fig. 21. The numbers near the corresponding curves show the values of $e\varphi/T \ln(50^2)$. The dashed line shows the equipotential surfaces obtained in the approximate solution of the Poisson equation and neglecting the influence of the electric field on the motion of the ions. It would be of interest to carry out a more detailed comparison of the results of[38] with the results obtained above (see Fig. 12) for a disc. Such a comparison is made difficult, however, by the fact that the publication[38] is not sufficiently detailed.

XV. EXPERIMENTAL INVESTIGATION OF THE PERTURBED ZONE IN THE VICINITY OF ROCKETS AND SATELLITES IN THE IONOSPHERE

Experimental investigations of the perturbations produced in the ionosphere by a satellite or by a rocket is of appreciable interest. The acquisition and reduction of the appropriate data is, however, a difficult task. Indeed, the diagnostics of a rarefied plasma is a complicated matter even under ordinary laboratory conditions. Added to these difficulties is the fact that the measurements are carried out on an object that moves in the ionosphere. The information must be accumulated and transmitted over a large distance. It is also important that the body usually executes a complicated motion in space. The position of the measuring instrument relative to the direction of motion of the body varies in time. It is therefore necessary to reduce the observation results very carefully, taking into account the exact position of the instrument relative to the direction of motion of the body at the instant of time when the measurement was performed. The number of papers containing such a detailed reduction of the observation data is small[33-36,39,40].

In comparing the experimental results with the theory, it should be borne in mind that the shape of the surface of the body, with allowance for the apparatus placed in it, is usually quite complicated. In addition, the conditions in the ionosphere vary strongly with altitude, and also with the time of the day, with the geographic latitude, etc. The dimensionless parameters characterizing the features of flow around the bodies vary accordingly.

1. Measurements on Rockets

K. Norman and A. P. Willmore[33] measured the flux of ions on the surface of a high altitude rocket. The rocket was launched in South Australia (Woomera) in the nighttime. The measurements were performed while the rocket moves at altitudes between 280 and 500 km. The rocket velocity changed accordingly from 3.0 to 2.2 km/sec. Besides the general motion, the rocket rotated about its axis with an angular velocity of 0.218 rad/sec and executed gyroscopic motion with a cone apex angle 89.8° and an angular velocity $\Omega = 0.144$ rad/sec. Because of this, the velocity component in the direction orthogonal to the rocket axis changed continuously in magnitude.

Four probes uniformly spaced 90° apart in a plane perpendicular to the cylinder axis were located on the surface of the rocket in the region where it could practically be regarded as a cylinder. The probes were flat discs of 5 cm radius. They were at a constant potential of −3.2V relative to the surface of the rocket. The total current of the ions to the probe was measured. The measured ion flux as a function of the angle θ between the position of the probe and the direction of the rocket velocity (more accurately, its component in the plane perpendicular to the cylinder axis) is shown in Fig. 22 (circles); here I_0 is the maximum flux, which occurs when $\theta = 0$.

Let us compare the results of the experiment and the calculation. At altitudes from 300 to 500 km at nighttime, one can assume that the ions are mainly O^+ with M = 16 (in proton-mass units). The ion temperature is close to the electron temperature and ranges from 900 to 1500°K (see[3]). Consequently, the quantity $b = (Mv_0^2/2T_e)^{1/2}$ ranged from 3.2 at 280 km to 1.8 at 500 km. On the average, $b \approx 2.5$. The ratio I/I_0 for the ion flux on the surface of the cylinder, calculated in accordance with formula (47) at b = 2.5, is shown in Fig. 22 by the dashed line. We see that at large angles $\theta > 50-60°$ the experimentally measured I/I_0 is much higher. It is natural to assume that the increase of the ion flux at large angles θ, as observed in the experiment, is connected with the influence exerted on the ion motion by the electric field of the probes.

Actually, the probes used in the experiment were not screened. Their potential relative to the surface of the body was −3.2 V, and relative to the plasma φ_0 was −(3.5—4) V. Consequently, under the experimental conditions the ratio $-e\varphi_0/T_e \approx 30-40$. The plasma

concentration measured in the same experiments varied in the range $(1-2.4)\times 10^5$ cm^{-3}. The average value was $N_0 \approx 2\times 10^5$ cm^{-3}. Consequently, the Debye radius was $D \approx 0.5$ and the ratio for the probe was $(R_0/D) \approx 10$. We see that $-e\varphi_0/T_e \sim (R_0/D)^{4/3}$. Under these conditions, as follows from the statements made in Sec. 5 of Ch. XIV, the ion flux to the probe at large angles θ should greatly increase as a result of the gathering action of the electric field of the probe. The calculated ratio I/I_0 in accordance with formula (97), i.e., with allowance for the gathering of the ions by the probe field, is shown in Fig. 22 by the solid curve (for $-e\varphi_0/T_e = 35$, $z_0/D = \sqrt{\pi R_0^2}/D \approx 17.7$, $b = 2.5$). The agreement between theory and experiment can be regarded as satisfactory.

In[33] they also measured the dependence of the ion flux to a probe located behind the body ($\theta \sim 180°$) on the velocity of the body. A comparison of these results for the theory, given in[16], has shown better agreement. However, in this calculation, as emphasized in[16], a rather crude approximation was used, namely, the cylindrical surface was replaced by its cross section, a plate (which is valid only at sufficiently large distances from the surface; see Ch. VIII); in addition, the gathering of the ions by the probe field was not taken into account. The results obtained by us make it possible to refine the calculation. The distribution of the ions behind the cylinder is described by formula (54). Calculation by means of (54) for the same values of the parameters as in[16] shows that the ion concentration on the surface of the cylinder at $\theta = 180°$ is smaller by a factor 10—20. On the other hand, allowance for the gathering of the ions by the probe field leads to an increase of the flux by a factor 6—10. Thus, the refined theory leads to values of $I(\theta = 180°)/I_0$ which are smaller by a factor 1.5—3 than those obtained with the approximate formula in[16]. In this case the result depends on the radius of the rocket, which is not indicated in[33]. In addition, the concentration of the flux of the ions increase very rapidly when the probe deviates from a position strictly on the axis behind the body (for example, when the angle θ changes by 10°, the concentration increases by 2—3 times). In the measurements, this position was not maintained with sufficient accuracy. Therefore, a detailed comparison of these measurements with the refined theory serves no purpose.

2. Measurements on the Satellite "Ariel-1"

The authors of[34-36] measured the densities of the ion and electron fluxes in the vicinity of the satellite "Ariel-1". The altitude of the moving satellite above the earth ranged from 390 to 1210 km, and the inclination of the orbit was 54°. The period of revolution of the satellite around the earth was 101 min. In addition, the satellite rotated about one of its axes at a rate of 35 rpm. The direction of the rotation axis remained almost constant in space, and the angle between this axis and the satellite velocity varied during the orbital motion. This resulted in a periodic variation of the probe positions relative to the direction of motion of the body.

Two probes measured the electron current. One of them (probe 1) was located on the surface of the

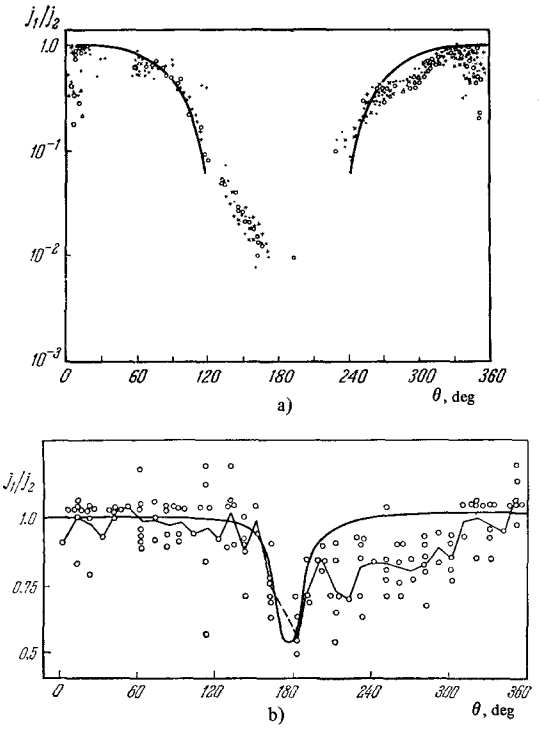

FIG. 23. Electron and ion concentration $n = N/N_0$ as a function of the angle θ between the direction of motion of the body and the radius vector drawn to the point under consideration. Circles—measurements of j_1/j_2: a) near the surface; b) at a distance $5R_0$.

satellite. The shape of the satellite was nearly spherical, with a radius $R_0 = 30$ cm. Probe 2 was located on a special rod and was located at a distance $5R_0$ from the center. The ratio of the flux j_1 to probe 1 to the flux j_2 to probe 2 is shown in Fig. 23a. The abscissas represent the angle θ characterizing the position of the probe 1 relative to the direction of motion of the satellite (the results shown in Fig. 23a represent the total of five days of measurement marked respectively by the symbols x, 0, ●, +).

In comparing the results of the experiment with the theory, we shall take into account the fact that the ratio of the electron fluxes is approximately equal to the concentration ratio $(j_1/j_2 = N_1/N_2)$. N_1 is equal to the concentration of the ions on the boundary of the double layer. It is natural to assume that the concentration N_2 is unperturbed, i.e., that it is equal to N_0. The value of $b = (Mv_0^2/2T_e)^{1/2}$ for the region where the satellite move ranged from $b \approx 6$ (at night in the perigee) to $b \approx 1.5$ (in the apogee). According to[36], the average value is $\bar{b} = 3.75$. The solid curve of Fig. 23a represents the ion concentration as calculated by formula (54) ($\sin^{-1}(R_0/z) = \pi/2$), which is valid near the surface of a sphere not too close to its axis, at approximately $\theta \lesssim 120°$ (and of course also at $\theta \gtrsim 240°$). The agreement between the theory and experiment in this region is satisfactory. At angles $\theta > 120°$, the dimension of the screening layer becomes noticeable. This is the start of the region of maximum rarefaction. A discussion of the measurements in this region is best carried out in the next section, where we present the results of experiments[39] in which more detailed data were obtained.

Figure 23b shows the results of measurements of the flux of electrons with the aid of probe 2, located at a distance $5R_0$ from the center, as a function of the angle θ between the directions of the probe and the direction of motion of the body. We see an appreciable scatter of the experimental points. The thin curve is the average result of the experiment. The thick curve is the result of a calculation of the ion concentration for b = 3.75 in accordance with the neutral-gas formula (i.e., neglecting the influence of the electric field on the ion motion)[2,37]. These formulas should be sufficiently accurate in the case under consideration, since $t = z/R_0 b \approx 1.2$, and at such large distances as indicated in Ch. IX, allowance for the influence of the electric field leads only to comparatively small change of the ion concentration. It is seen from Fig. 23b that a definite correspondence exists between the results of the measurements in the calculation: the position and the width of the principal minimum, and also the value of the concentration at the minimum, agree with the theory*. It should be noted that an appreciable contribution to the perturbation is made at a distance $5R_0$ from the center of the satellite not only by the body of the satellite, but also by several other elements located near the satellite[36]. It is possible that this is the cause of the complicated and strongly fluctuating picture of the experimental points shown in Fig. 23. It is also important that consideration of only the average Mach number is a very crude approximation. Actually, the value of b changes strongly with altitude, owing to the change of the ionic composition and of the temperature of the ionosphere. This strongly influences the structure of the perturbed zone. For a more accurate comparison of theory and experiment, it is therefore necessary to perform the measurements at different altitudes separately, and that these measurements be accompanied where possible by complete data on the structure of the unperturbed ionosphere, such as the relative concentration of the different ions (O^+, H^+, He^+), the temperatures of the electrons and the ions, and the electron concentration.

In[34] there were also observed oscillations of the particle fluxes to the probes; they were interpreted as the results of oscillations in the plasma. The oscillations were localized in the region of the boundary of the wake (the experimental accuracy inside the wake is insufficient to establish the presence or absence of oscillations). Their frequency ranged from 2.7 to 3.7 kHz. The instability indicated in Ch. XI leads to excitation in the plasma of oscillations with frequencies $f \sim \Omega_0/2\pi = (e^2N^0/\pi M)^{1/2}$ (in the coordinate system of the satellite). At $N_0 = 10.5$ and M = 16 we obtain $f \approx 5$ kHz. We can thus assume that the aforementioned ion-acoustic instability of the plasma in the region of the weight of the body was observed in these experiments.

3. Measurements on the Satellite "Explorer-31"

A preprint by U. Samir and G. L. Wrenn[39] contains the results of measurements of the flux of electrons on the satellite "Explorer-31" in December 1965–January 1966. The inclination of the orbit was 80°, and the altitude above the earth's surface ranged from 500 to 3000 km. The satellite had the form of an octagonal parallelepiped; it can be approximately regarded as a cylinder 1 m high and of radius $R_0 \sim 0.5$ m. The satellite rotated around the axis of the parallelepiped, which was stabilized orthogonally to the orbit.

The electron disc probe of radius 1 cm was mounted on one of the side faces at a distance of 20 cm from the lower edge of the satellite. The electron flux measured by the probe, as a function of the angle θ between the velocity of the body and the direction from the axis to the probe, is shown in Figs. 24a–e. The ordinates represent the ratio $j(\theta)/j_0$, where j_0 is the maximum flux, which is produced when the direction to the probe coincides to the direction of the body velocity ($\theta = 0$). The circles show the experimental results. The measurements were made at different altitudes h and at different local times t, as indicated in the figures. Simultaneously, an ion spectrometer was used to measure the average ion mass $\overline{M}$. Assuming for simplicity that the ionospheric plasma at the altitudes under consideration contains only O^+ and H^+ ions, we can determine from the value of $\overline{M}$ the relative concentration of these ions: $n_{H^+} = (16 - \overline{M})/15$ and $n_{O^+} = 1 - n_{H^+}$.

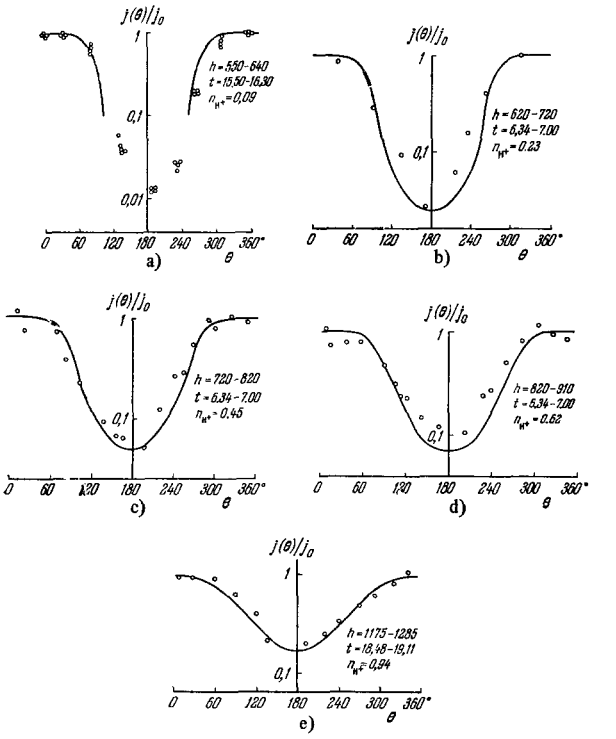

FIG. 24. Concentration of the electrons and ions $n = N/N_0$ in the quasineutral region at the surface of the body as a function of the angle θ. Circles—results of measurements of j/j_0.

*The statement made in [36] that there is an appreciable discrepancy (by a factor of 5) between the results of the experiment in question and the formulas of the neutral-approximation theory [37] is the consequence of a misunderstanding. Apparently, the authors of [36] compared the results of a calculation for b = 8 with the results of an experiment for b = 3.75. When b = 3.75 and $z = 5\ R_0$ we obtain from Table 2 of [37] $N/N_0 = 0.53$, in agreement with experiment, whereas at b = 8 the value of N/N_0 is actually smaller by a factor of 5–6.

The average value of n_{H^+} is also indicated in the figures.

At an altitude $h \lesssim 600$ km, the oxygen ions constitute the overwhelming majority. In this case it is possible to neglect the influence of the small admixture of hydrogen everywhere except in the region of strong rarefaction. The solid curve in Fig. 24a shows the concentration of the oxygen ions $N(\theta)/N_0$, calculated by means of formula (54) ($T_e = 2000°$, $b_{O^+} = 5.3$, $\sin^{-1}(R_0/z) = \pi/2$). The agreement between the theoretical curves and experiment outside the region of maximum rarefaction ($\theta < 120°$) is satisfactory (similar measurements performed on the satellite "Ariel-1" are shown in Fig. 23a).

An angles $\theta > 120°$, as already noted above, the dimension of the screening layer becomes noticeable. This is where the region of maximum rarefaction begins. In comparing the results of the measurements with the theory in the region of maximum rarefaction, it is necessary to take into account the following circumstances. First, the concentration of the ions in the region of maximum rarefaction is much smaller than the concentration of the electrons[37,2,38]. They become comparable only on the boundary of this region. Consequently, the electron flux measured by the probe in the region $\theta > 120°$ corresponds to the plasma concentration on the boundary of the region of maximum rarefaction, which is quite far from the surface of the body. Let us consider, for example, the case when the probe is situated exactly behind the satellite ($\theta = 180°$). This case is shown in Fig. 25 (side view). The boundary of the region of maximum rarefaction in the vicinity of the probe is shown dashed in the figure. It can be characterized by the angle φ_0. An approximate calculation shows that for the conditions considered here the angle φ_0 amounts to approximately 35–50°, On the average, it can be assumed to equal 45°.

Further, in the region of maximum rarefaction, the relative concentration of the hydrogen ions increases strongly. Let us recognize that at $T_e \sim 1500$–$3000°K$ and $v_0 = 7.6 \times 10^5$ cm/sec we have $b_{O^+} \sim 4.5$–6 for oxygen and $b_{H^+} \sim 1.1$–1.5 for hydrogen. It then follows from the results of Ch. IV that whereas $n_{H^+} > (0.01$–$0.05)$ in the unperturbed ionospheric plasma, in the region of the maximum rarefaction the hydrogen ions are in the majority. Therefore in all the cases considered in the present section the structure of the region of maximum rarefaction is determined by the hydrogen ions. This is confirmed by the data of Samir and Wrenn. Indeed, the electron temperature and altitude 600–900 km, changes on the average from 2000 to 3000°K. Accordingly, the Mach number for the hydrogen ions is $b_{H^+} = 1.3$–1.1. We see that the parameter b_{H^+} changes insignificantly. A much stronger change takes place in the relative condensation of the hydrogen ions n_{H^+}, namely from 3–5% to 60%. Consequently, in the indicated region of altitudes the experimentally measured ratio $j(\theta = 180°)/j_0$ should increase in proportion to the concentration of the hydrogen ions n_{H^+}. This ratio, as seen from Fig. 26, actually holds true.

It is important that the value of the Mach number for the hydrogen ions is low, $b_{H^+} \sim 1$–1.5. In this case it follows from the results obtained in Chs. III and X that the influence of the electric field on the motion of the ions in a quasineutral plasma is not very strong and can be neglected in the approximation. In addition, at not too small values of $n_{H^+} \gtrsim 20\%$, the electric field has likewise an insignificant influence on the heavy oxygen ions (see Ch. IV, formula (46)). Therefore to calculate the concentration of the plasma at $n_{H^+} \gtrsim 20\%$ it is possible to use the formulas of the neutral approximation[2]. Recognizing that in this approximation the different ion components of the plasma are independent, we find that the plasma concentration on the boundary of the region of maximum rarefaction is equal to

$$\frac{N(\theta)}{N_0} = n_{O^+}\frac{1+\Phi(b_{O^+}\cos\varphi_0\cos\theta)}{1+\Phi(b_{O^+}\cos\varphi_0)} + n_{H^+}\frac{1+\Phi(b_{H^+}\cos\varphi_0\cos\theta)}{1+\Phi(b_{H^+}\cos\varphi_0)}; \quad (98)$$

Here $\Phi(z)$ is the probability integral and φ_0 is an angle characterizing the position of the boundary of the region of maximum rarefaction (see Fig. 25). Formula (98) describes in the neutral approximation the distribution of the ions on the surface of a body of revolution with angle φ_0 between the axis and the generatrix. Strictly speaking, it would be necessary to take into account the fact that the angle φ_0 decreases with decreasing φ. Therefore, for example, on the frontal surface of the body we have $\varphi_0 \sim 0$. This change of φ_0, however, leads only to an insignificant change in the concentration $N(\theta)$, lying within the limits of accuracy of formula (96). We can therefore regard the angle φ_0 as a constant, determined for the angle $\theta = 180°$. In our case, as indicated above, the average value is $\varphi_0 \sim 45°$.*

The result of the calculation of the ratio $N(\theta)/N_0$ for $\varphi_0 = 45°$ is shown by the solid curves in Figs. 24b–e, where it was assumed that $T_e = 2000°K$ and $v_0 = 7.6 \times 10^5$ cm/sec; for Fig. 24e it was assumed that $T_e = 3000°K$ and $v_0 = 7.5 \times 10^5$ cm/sec. The agreement with experiment is seen to be satisfactory. The straight line in Fig. 26 is plotted in accordance with formula (98) for $\theta = 180°$ ($T_e = 2500°K$ and $v_0 = 7.6 \times 10^6$ cm/sec). The dashed curve takes into account the change of the electron temperature and of the velocity

FIG. 25. Location of probe behind the body. Dashed line–limit of quasineutral region in the vicinity of the probe.

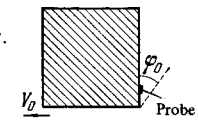

FIG. 26. Electron and ion concentration equals N/N_0 on the boundary of the quasineutral region vs. the hydrogen ion concentration $n = N_{H+}/N_0$ (curves). Circle–results of measurements of $j(\theta = 180°)/j_0$.

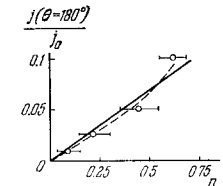

*Of course, the foregoing analysis is valid only for not too highly charged a body. More accurately, it is necessary to satisfy the condition $|\varphi_0| \ll (T_e/e)(R_0/D)^{4/3}$, where φ_0 is the potential of the surface of the body, R_0 is its characteristic dimension, are $D = \sqrt{T_e/4\pi e^2 N_0}$ is the Debye radius in the unperturbed plasma. At altitudes h ~ 2000–3000 km, this condition is no longer satisfied.

v_0 (it was assumed that T_e increases linearly from 2000°K at 600 km altitude to 3000°K at 1000 km).

[1] Ya. L. Al'pert, A. V. Gurevich, and L. P. Pitaevskiĭ, Usp. Fiz. Nauk 79, 23 (1963) [Sov. Phys.-Usp. 6, 13 (1963)].
[2] Ya. L. Al'pert, A. V. Gurevich, and L. P. Pitaevskiĭ, Iskusstvennye sputniki v razreshennoĭ plazme (Artificial Satellites in a Rarefied Plasma), Nauka, 1964.
[3] W. E. Gordon, F. Region and Magnetosphere, Report on XV Assembly of URSI, Munich, 1966.
[4] A. V. Gurevich and L. P. Pitaevskiĭ, Geomagnetizm i aeronomiya 4, 817 (1964).
[5] M. Kaminskii, Atomic and Ionic Collisions on Metal Surfaces (Russ. transl.), Mir, 1967.
[6] Yu. M. Panchenko and L. P. Pitaevskiĭ, Geomagnetizm i aéronomiya 4, 256 (1964).
[7] V. V. Vas'kov, Zh. Eksp. Teor. Fiz. 50, 1124 (1966) [Sov. Phys.-JETP 23, 748 (1966)].
[8] G. G. Chernyĭ, Techenie gaza s bol'shoĭ sverkhzvukovoĭ skorost'yu (Gas Flow with Large Supersonic Velocity), Fizmatgiz, 1959.
[9] A. V. Gurevich, L. V. Pariĭskaya, and L. P. Pitaevskiĭ, Zh. Eksp. Teor. Fiz. 49, 647 (1965) [Sov. Phys.-JETP 22, 449 (1966)].
[10] A. V. Gurevich and L. P. Pitaevskiĭ, ibid. 56, 1778 (1969) [29, 954 (1969)].
[11] L. D. Landau and E. M. Lifshitz, Mekhanika sploshnykh sred, Gostekhizdat, 1954 [Fluid Mechanics, Addison-Wesley, 1958].
[12] A. V. Gurevich, L. V. Pariĭskaya, and L. P. Pitaevskiĭ, Zh. Eksp. Teor. Fiz. 54, 891 (1966) [Sov. Phys.-JETP 27, 593 (1966)].
[13] N. I. Bud'ko, Geomagnetizm i aéronomiya 6, 1008 (1966).
[14] A. V. Gurevich and V. V. Smirnova, ibid. 9, No. 6 (1969).
[15] V. V. Smirnova, ibid. 9, No. 6 (1969).
[16] A. V. Gurevich and L. P. Pitaevsky, Phys. Rev. Lett. 15, 346 (1965).
[17] L. D. Landau, Zh. Eksp. Teor. Fiz. 16, 574 (1946).
[18] V. N. Faddeeva and N. M. Terent'ev, Tablitzy integrala veroyatnosteĭ (Tables of Probability Integral), Gostekhizdat, 1954.
[19] V. G. Kurt and V. I. Moroz, Iskusstvennye sputniki Zemli 7, 78 (1961).
[20] D. B. Beard and F. S. Johnson, J. Geophys. Res. 66, 4113 (1961).
[21] E. C. Whipple, Jr., Preprint X-615, 65-296, Goddard Space Flight Center, 1965.
[22] V. V. Smirnova, Geomagnetizm i aéronomiya 6, 276 (1966).
[23] L. Jaffe and J. Rittenhouse, in: Raketnaya tekhnika (Rocket Engineering—translations), No. 3, 7 (1962).
[24] F. J. F. Osborne, M. P. Bachynski, and M. A. Kasha, Preprint 6-2-6, URSI Spring Meeting, Washington, 1965.
[25] M. A. Kasha, F. J. F. Osborne, T. W. Johnston, and I. P. Shkarofsky, Proc. 2nd Symposium on Interaction of Space Vehicles with Ionized Atmosphere, Miami, 1965.
[26] A. V. Gurevich, Kosmicheskie issledovaniya 2, 68 (1964).
[27] M. V. Maslennikov and Yu. S. Sigov, Dokl. Akad. Nauk SSSR 159, 1013 (1964) [Sov. Phys.-Dokl. 9, 1063 (1965)].
[28] J. C. Taylor, Planet. and Space Sci. 15, 155, 463 (1967).
[29] E. C. Walker, Interaction of Space Vehicles with an Ionized Atmosphere (S. F. Singer, ed.), Pergamon Press, N. Y., 1965.
[30] J. Langmuir and K. Blodgett, Phys. Rev. 22, 347 (1923); 24, 49 (1924).
[31] A. M. Moskalenko, Geomagnetizm i aéronomiya 4, 260 (1964); 11, 383 (1965).
[32] V. S. Knyazyuk and A. M. Moskalenko, ibid. 6, 997 (1966).
[33] K. Norman and A. P. Willmore, Planet. and Space Sci. 13, 1 (1965).
[34] P. I. Bowen, R. L. F. Boyd, C. L. Henderson, and A. P. Willmore, Proc. Roy. Soc. A281, 514 (1964).
[35] U. Samir and A. P. Willmore, Planet. and Space Sci. 13, 285 (1965).
[36] C. L. Henderson and U. Samir, Planet. and Space Sci. 15, 1499 (1967).
[37] A. V. Gurevich, Iskusstv. sputniki zemli (Artif. Earth Satellites) 10 (7), 101 (1961).
[38] V. Liu and H. Jew, Rarefied Gas Dynamics (C. L. Brundin, Ed.), N. Y. 1967, p. 1703.
[39] U. Samir and G. L. Wrenn, The Dependence of Charge and Potential Distribution around Spacecraft on Ionic Composition. Preprint, 1969.
[40] V. N. Borovenko, Kosmicheskie issledovaniya 5, 58 (1967).

ADDITIONAL LITERATURE

Reviews

[41] R. E. Bourdeau, Space Sci. Rev. 1, 716 (1962/63).
[42] Ya. L. Al'pert, Space Sci. Rev. 4, 373 (1965).
[42a] G. Fournier, Interactions d'un satellite avec l'ionosphere et applications aux problemes de trainees et de nesures par sondes. Preprint O.N.E.R.A., Note Techn. Nr. 142 (1969).

Technical Papers

[43] S. H. Lam and M. Greenblatt, AIAA Journ. 3, 1850 (1965).
[44] V. C. Liu, Nature 208, 883 (1965); 215, 127 (1967).
[45] V. S. Pan and R. Vaglio-Laurin, AIAA Journ. 5, 1801 (1967).
[46] V. V. Vas'kov, Geomagnetizm i aéronomiya 6, 1104 (1966).
[47] V. I. Karpman, Zh. Eksp. Teor. Fiz. 52, 1657 (1967) [Sov. Phys.-JETP 25, 0000 (1967)].
[48] D. J. Prager and M. L. Rasmussen, Preprint SUDAAR No. 299, 1967.
[49] S. D. Drell, H. M. Foley, and M. A. Ruderman, J. Geophys. Res. 70, 3131 (1965).
[50] L. W. Parker and B. L. Murphy, J. Geophys. Res. 72, 1631 (1967).

Scattering of Radio Waves by the Trail of a Body

[51] A. V. Gurevich and L. P. Pitaevskiĭ, Geomagnetizm i aéronomiya 6, 842 (1966).
[52] Yu. K. Kalinin, ibid. 5, 289 (1965).
[53] S. Rand and F. Albini, AIAA Journ. 5, 1174 (1967).
[54] Booker, J. Geophys. Res. 66, 1073 (1961).
[55] V. V. Vas'kov, Geomagnetizm i aéronomiya 8, 778 (1968).

Measurements in the Ionosphere

[56] I. M. Imyanitov, G. L. Gdalevich, and Ya. M. Shvarts, Iskusstvennye sputniki zemli 17, 67 (1963).
[57] R. E. Bourdeau and J. Donlly, Proc. Roy. Soc. A281, 487 (1964).
[58] F. L. Scarf, G. M. Crook, and R. W. Fredirics, J. Geophys. Res., 70, 3045 (1965); Radio Sci. 1, 939 (1965).
[59] R. L. F. Boyd, Space Sci. Rev. 7, 230 (1967).
[60] U. Fahleson, Space Sci. Rev. 7, 238 (1967).
[61] V. V. Afonin, T. K. Borus, G. L. Gdalevich, B. N. Gorozhankin, K. I. Gringauz, R. E. Rybchinskii, and N. M. Shyutte, in: Issledovaniya kosmicheskogo prostranstva (Outer Space Research), Nauka, 1965, p. 151.
[62] K. I. Gringauz, B. N. Gorozhankin, N. M. Shyutte, and G. L. Gdalevich, Dokl. Akad. Nauk SSSR 151, 560 (1963).
[63] N Kawashima and K. Hirao, Preprint JAERT No. 2551 (Japan), Ibaraki, 1966.
[64] V. Fiala and L. R. O. Storey, Preprint GRI, NTR/32 (France), Saunt Mour des Foses, 1968.
[65] G. W. Sharp, W. B. Hanson, and D. D. McKibben, Techn. Rept. 6-90-63-53, 1963.

Laboratory Experiments

[66] W. A. Clayden, Rarefied Gas Dynamics, Academic Press, 1964, p. 435.
[67] W. A. Clayden and C. V. Hurdle, Rarefied Gas Dynamics (G. L. Brundin Ed.), Academic Press, 1966, p. 1717.
[68] E. D. Knechtell and W. G. Pitts, AIAA Journ. 2, 1148 (1964).
[69] F. J. F. Osborne, URSI Spring Meeting, Washington, Preprint 3-8-6, 1965.
[70] P. F. Hall, R. F. Kemp, and J. M. Sellen, AIAA Journ. 2, 1032 (1964).
[71] P. J. Barret, Phys. Rev. Lett. 13, 742 (1964).
[72] N. Kawashima and S. Mori, Phys. Fluids 9, 700 (1966).
[73] N. Kawashima and S. Mori, AIAA Journ. 6, 110 (1968).
[74] N. Kawashima, J. Geophys. Res. 20, 3203 (1965).
[75] S. D. Hester and A. A. Sonin, Rarefied Gas Dynamics, Preprint, 1968.
[76] V. V. Skvortsov and L. V. Nosachev, Kosmicheskie issledovaniya 6, 228, 855 (1968).

Translated by J. G. Adashko